We are IntechOpen, the world's leading publisher of Open Access books Built by scientists, for scientists

4,800
Open access books available

122,000
International authors and editors

135M
Downloads

Our authors are among the

154
Countries delivered to

TOP 1%
most cited scientists

12.2%
Contributors from top 500 universities

CLARIVATE ANALYTICS BOOK CITATION INDEX INDEXED

WEB OF SCIENCE™

Selection of our books indexed in the Book Citation Index in Web of Science™ Core Collection (BKCI)

Interested in publishing with us?
Contact book.department@intechopen.com

Numbers displayed above are based on latest data collected.
For more information visit www.intechopen.com

6

Vehicle Stability Enhancement Control for Electric Vehicle Using Behaviour Model Control

Kada Hartani and Yahia Miloud
Electrical Engineering Departmant,
University of Saida
Algeria

1. Introduction

In this chapter, two permanent magnet synchronous motors which are supplied by two voltage inverters are used. The system of traction studied Fig.1, belongs to the category of the multi-machines multi-converters systems (MMS). The number of systems using several electrical machines and/or static converters is increasing in electromechanical applications. These systems are called multi-machines multi-converters systems (Bouscayrol, 2003). In such systems, common physical devices are shared between the different energetic conversion components. This induces couplings (electrical, mechanical or magnetic) which are quite difficult to solve (Bouscayrol, 2000).
The complexity of such systems requires a synthetic representation in which classical modeling tools cannot always be obtained. Then, a specific formalism for electromechanical system is presented based on a causal representation of the energetic exchanges between the different conversion structures which is called energetic macroscopic representation (EMR). It has developed to propose a synthetic description of electromechanical conversion systems. A maximum control structure (MCS) can be deduced by from EMR using inversion rules. The studied MMS is an electric vehicle. This system has a mechanical coupling, Fig.1. The main problem of the mechanical coupling is induced by the non-linear wheel-road adhesion characteristic. A specific control structure well adapted to the non-linear system (the Behaviour Model Control) is used to overcome this problem. The BMC has been applied to a non-linear process; therefore, the wheel-road contact law of a traction system can be solved by a linear model.
The control of the traction effort transmitted by each wheel is at the base of the command strategies aiming to improve the stability of a vehicle. Each wheel is controlled independently by using an electric motorization. However, the traditional thermal motorization always requires the use of a mechanical differential to ensure the distribution of power on each wheel. The mechanical differential usually imposes a balanced transmitted torques. For an electric traction system, this balance can be obtained by using a multi-motor structure which is shown in Fig.1. An identical torque on each motor is imposed using a fuzzy direct torque control (FDTC) (Miloudi, 2004; Tang, 2004; Sun, 2004, Miloudi, 2007). The difficulty of controlling such a system is its highly nonlinear character of the traction forces expressions. The loss of adherence of one of the two wheels which is likely to destabilize the vehicle needs to be solved in this chapter.

2. Presentation of the traction system proposed

The proposed traction system is an electric vehicle with two drives, Fig.1. Two machines thus replace the standard case with a single machine and a differential mechanical. The power structure in this paper is composed of two permanent magnet synchronous motors which are supplied by two three-phase inverters and driving the two rear wheels of a vehicle through gearboxes, Fig. 2. The traction system gives different torque to in-wheel-motor, in order to improve vehicle stability. However, the control method used in this chapter for the motors is the fuzzy direct torque control with will give the vehicle a dynamic behaviour similar to that imposed by a mechanical differential (Arnet, 1997; Hartani, 2005; Hartani, 2007). The objective of the structure is to reproduce at least the behaviour of a mechanical differential by adding to it a safety anti skid function.

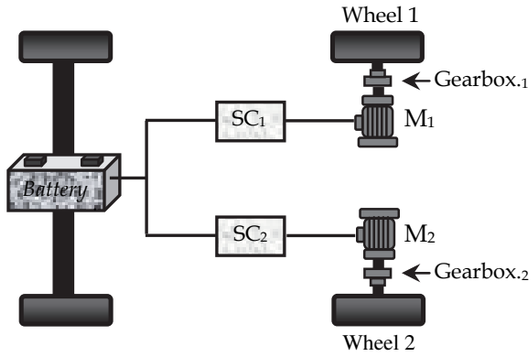

Fig. 1. Configuration of the traction system proposed

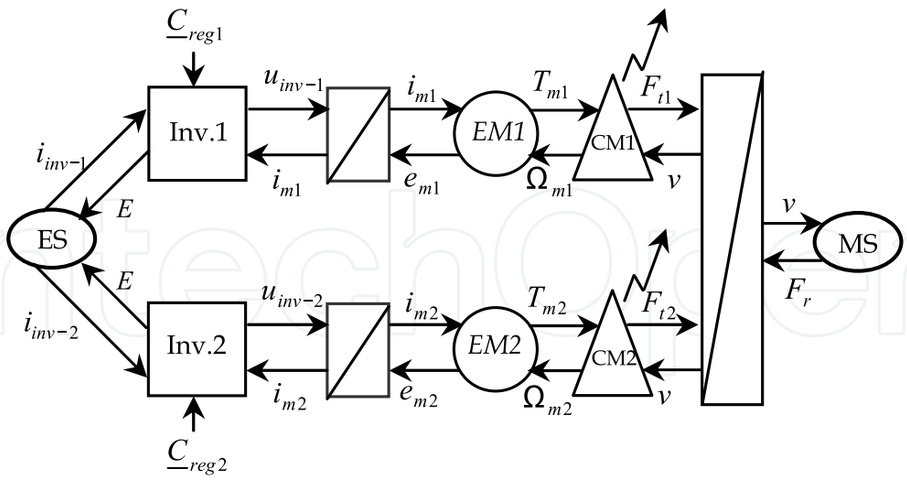

Fig. 2. EMR of the studied traction chain

2.1 Energetic macroscopic representation of the traction system

The energetic macroscopic representation is a synthetic graphical tool on the principle of the action and the reaction between elements connected (Merciera, 2004). The energetic macroscopic representation of the traction system proposed, Fig. 3, revealed the existence of

only one coupling called overhead mechanical type which is on the mechanical part of the traction chain.
The energetic macroscopic representation of the mechanical part of the electric vehicle (EV) does not take into account the stated phenomenon. However, a fine modeling of the contact wheel-road is necessary and will be detailed in the following sections.

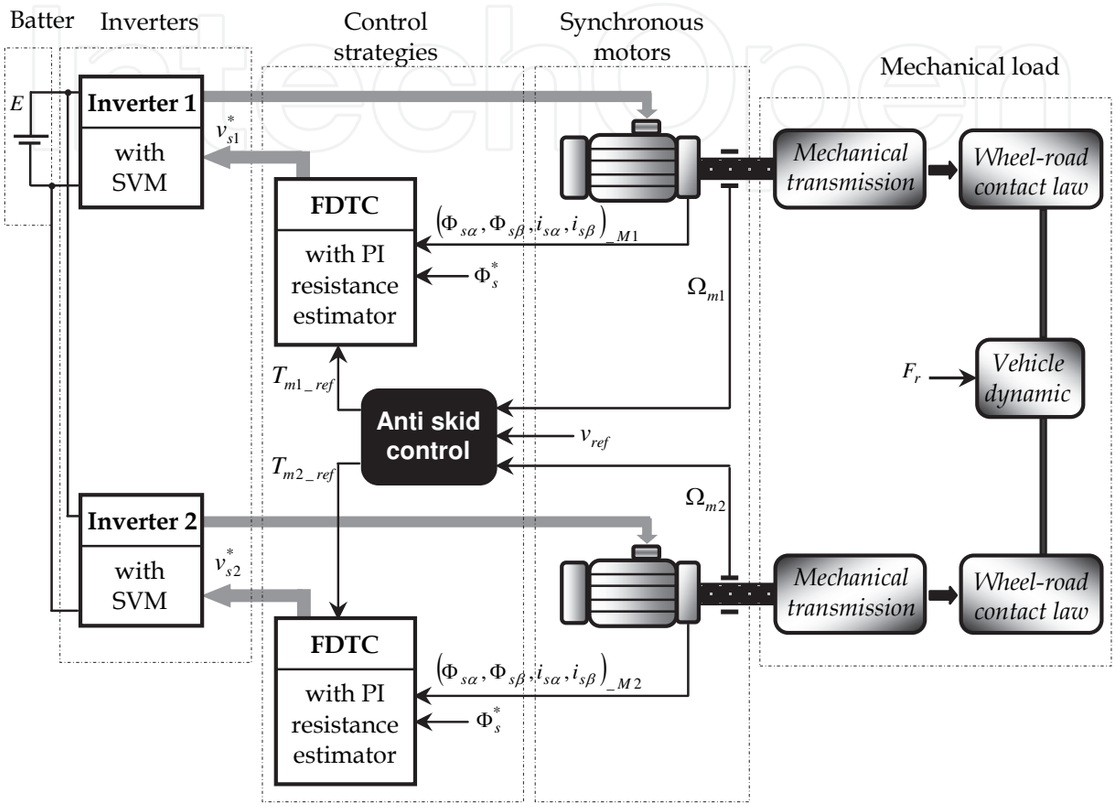

Fig. 3. Components of the traction system proposed

2.2 Traction motor model

The PMSM model can be described in the stator reference frame as follows (Pragasen, 1989):

$$\begin{cases} \dfrac{di_{s\alpha}}{dt} = -\dfrac{R_s}{L_s} i_{s\alpha} + \dfrac{\Phi_f}{L_s} \omega_m \sin\theta + \dfrac{1}{L_s} v_{s\alpha} \\ \dfrac{di_{s\beta}}{dt} = -\dfrac{R_s}{L_s} i_{s\beta} - \dfrac{\Phi_f}{L_s} \omega_m \cos\theta + \dfrac{1}{L_s} v_{s\beta} \\ \dfrac{d\omega_m}{dt} = -\dfrac{f}{J} \omega_m + \dfrac{p}{J}\left(T_{em} - T_{rm}\right) \end{cases} \quad (1)$$

and the electromagnetic torque equation

$$T_{em} = \frac{3}{2} p\Phi_f \left(-i_{s\alpha} \sin\theta + i_{s\beta} \cos\theta\right) \quad (2)$$

2.3 Inverter model

In this electric traction system, we use a voltage inverter to obtain three balanced phases of alternating current with variable frequency. The voltages generated by the inverter are given as follows:

$$\begin{bmatrix} v_a \\ v_b \\ v_c \end{bmatrix} = \frac{E}{3}\begin{bmatrix} 2 & -1 & -1 \\ -1 & 2 & -1 \\ -1 & -1 & 2 \end{bmatrix}\begin{bmatrix} S_a \\ S_b \\ S_c \end{bmatrix} \tag{3}$$

2.4 Mechanical transmission modeling of an EV

2.4.1 Modeling of the contact wheel-road

The traction force between the wheel and the road, Fig. 4(a), is given by

$$F_t = \mu N \tag{4}$$

where N is the normal force on the wheel and μ the adhesion coefficient. This coefficient depends on several factors, particularly on the slip λ and the contact wheel-road characteristics (Gustafsson, 1997; Gustafsson, 1998), Fig. 4(b). For an accelerating vehicle, it is defined by (Hori, 1998):

$$\lambda = \frac{v_\Omega - v}{v_\Omega} \tag{5}$$

The wheel speed can be expressed as:

$$v_\Omega = r\Omega \tag{6}$$

where Ω is the wheel rotating speed, r is the wheel radius and v is the vehicle speed. When $\lambda = 0$ means perfect adhesion and $\lambda = 1$ complete skid.

Principal non-linearity affecting the vehicle stability is the adhesion function which is given by Eq. (7) and represented on Fig. 4(b).

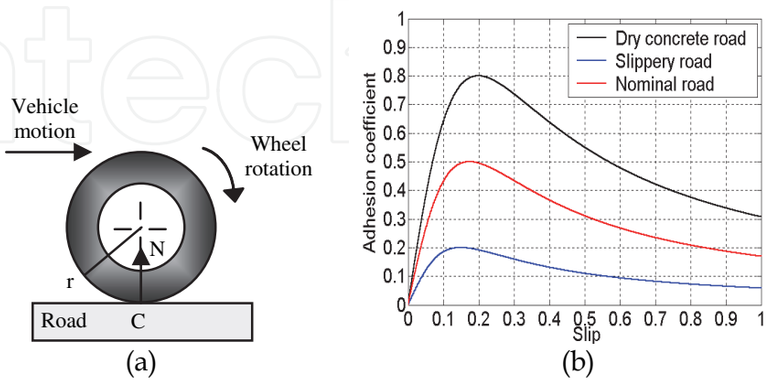

Fig. 4. (a) One wheel model, (b) contact wheel-road characteristics.

We now represent in the form of a COG (Guillaud, 2000) and an EMR, the mechanical conversion induced by the contact wheel-road, Fig. 5.

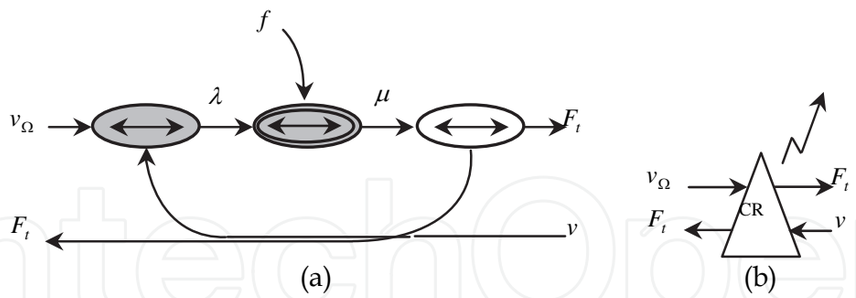

Fig. 5. Modeling of the contact wheel-road: (a) COG and (b) EMR.

2.4.2 Modeling of the transmission gearbox-wheel

Modeling of the transmission gearbox-wheel is carried out in a classical way which is given by:

$$\begin{cases} v_\Omega = r\Omega \\ T_r = rF_t \end{cases} \tag{7}$$

$$\begin{cases} \Omega = k_{red}\Omega_m \\ T_{rm} = k_{red}T_m \end{cases} \tag{8}$$

where r is the wheel radius, k_{red} the gearbox ratio, T_r the transferred resistive torque on the wheel shafts and T_{rm} the transferred resistive torque on the motor axle shafts, Fig. 6.

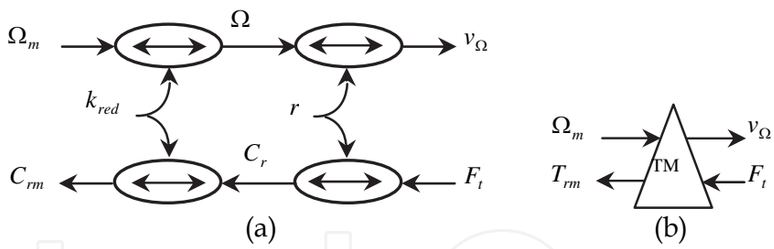

Fig. 6. Modeling of the mechanical drive: (a) COG and (b) EMR.

2.4.3 Modeling of the environment

The external environment is represented by a mechanical source (MS) on Fig. 3, leading to the resistance force of the vehicle motion F_r (Ehsani, 1997), where:

$$F_r = F_{aero} + F_{roll} + F_{slope} \tag{9}$$

F_{roll} is the rolling resistance, F_{aero} is the aerodynamic drag force and F_{slope} is the slope resistance.

The rolling resistance is obtained by Eq. (10), where μ_r is the rolling resistance coefficient, M is the vehicle mass and g is the gravitational acceleration constant.

$$F_{roll} = \mu_r Mg \tag{10}$$

The resistance of the air acting upon the vehicle is the aerodynamic drag, which is given by Eq. (11), where ρ is the air density, C_D is the aerodynamic drag coefficient, A_f is the vehicle frontal area and v is the vehicle speed (Wong, 1993).

$$F_{aero} = \frac{1}{2}\rho C_D A_f v^2 \tag{11}$$

The slope resistance and down grade is given by Eq. (12)

$$F_{slope} = Mgp_{\%} \tag{12}$$

2.5 EMR of the mechanical coupling

The modeling of the phenomenon related to the contact wheel-road enables us to separate the energy accumulators of the process from the contact wheel-road. However, the energy accumulators which are given by the inertia moments of the elements in rotation can be represented by the total inertia moments of each shaft motor J_Ω and the vehicle mass M, where:

$$J_\Omega \frac{d\Omega_m}{dt} = T_m - T_{rm} - f\Omega_m \tag{13}$$

and

$$M\frac{dv}{dt} = F_{t1} + F_{t2} - F_r \tag{14}$$

F_{t1}, F_{t2} are the traction forces developed by the left and right wheels and F_r is the resistance force of the motion of the vehicle.

The final modeling of the mechanical transmission is represented by the EMR, Fig. 7.

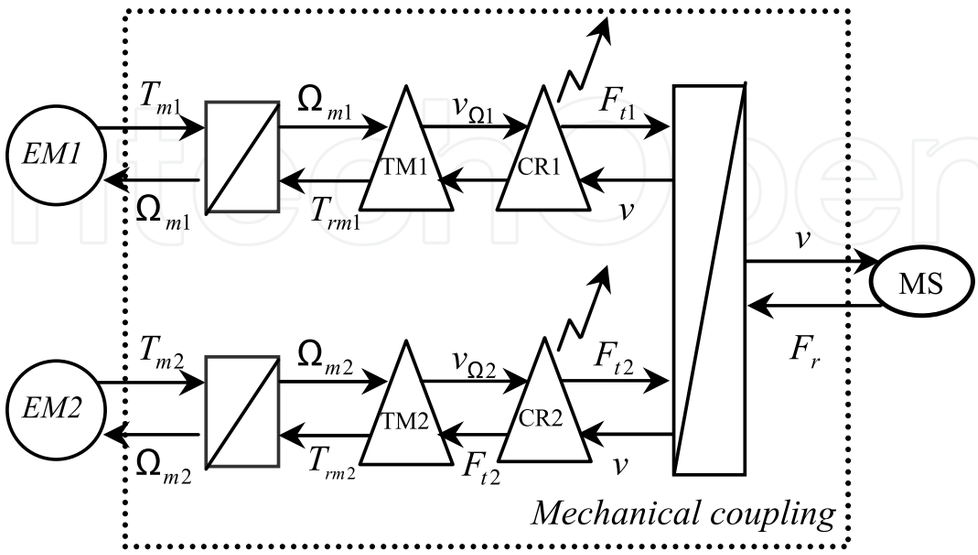

Fig. 7. Detailed EMR of the mechanical coupling

3. Control strategy

3.1 Fuzzy direct torque control

A fuzzy logic method was used in this chapter to improve the steady-state performance of a conventional DTC system. Fig. 8 depicts schematically a direct torque fuzzy control, in which the fuzzy controllers replace the flux linkage and torque hysteresis controllers and the switching table normally used in conventional DTC system (Takahachi, 1986; French, 1996; Vyncke, 2006; Vasudevan, 2004).

The proposed fuzzy DTC scheme uses the stator flux amplitude and the electromagnetic torque errors through two fuzzy logic controllers (i.e., FLC1 and FLC2) to generate a voltage space vector V_s^* (reference voltage); it does so by acting on both the amplitude and the angle of its components, which uses a space vector modulation to generate the inverter switching states. In Fig. 8 The errors of the stator flux amplitude and the torque were selected as the inputs, the reference voltage amplitude as the output of the fuzzy logic controller (FLC1), and the increment angle as the output of the fuzzy logic controller (FLC2) that were added to the angle of the stator flux vector. The results were delivered to the space vector modulation, which calculated the switching states S_a, S_b, and S_c.

The Mamdani and Sugeno methods were used for the fuzzy reasoning algorithms in the FLC1 and FLC2, respectively. Figs. 9 and 10 show the membership functions for the fuzzy logic controllers FLC1 and FLC2, respectively. Fig. 11 shows the fuzzy logic controller structure.

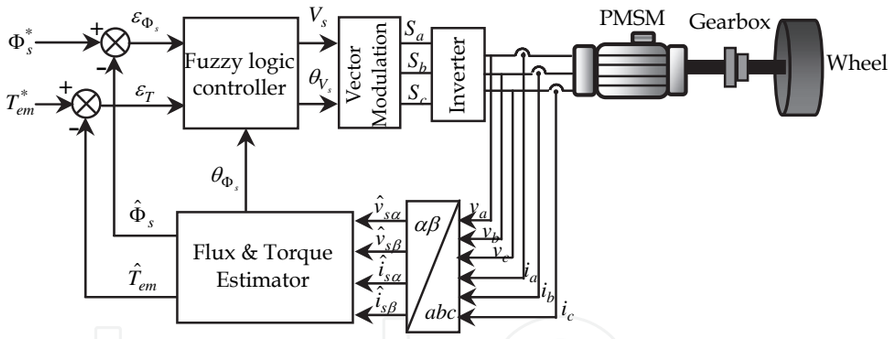

Fig. 8. System diagram of a PMSM-fuzzy DTC drive system with stator PI resistance estimator

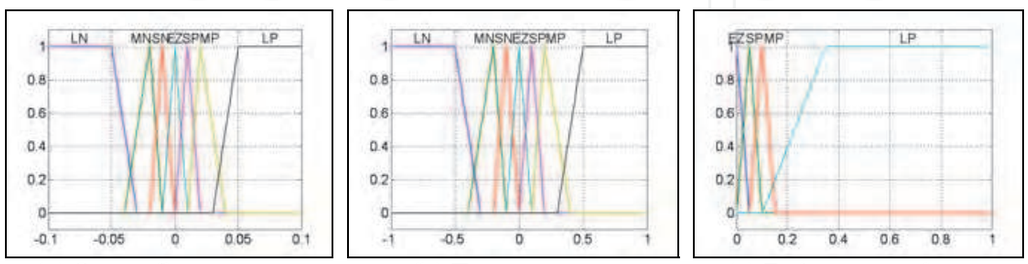

(a) Stator flux error (b) Torque error (c) Reference voltage

Fig. 9. Membership functions for the FLC1

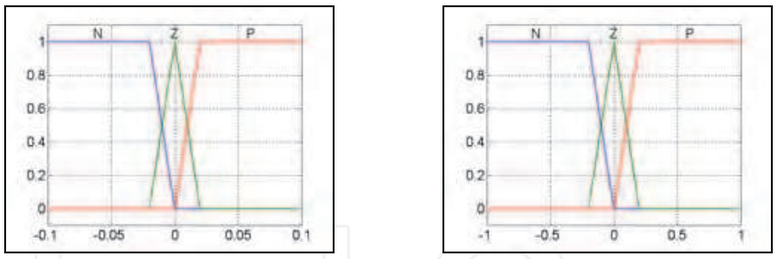

(a) Stator flux error (b) Torque error

Fig. 10. Membership functions for the FLC2

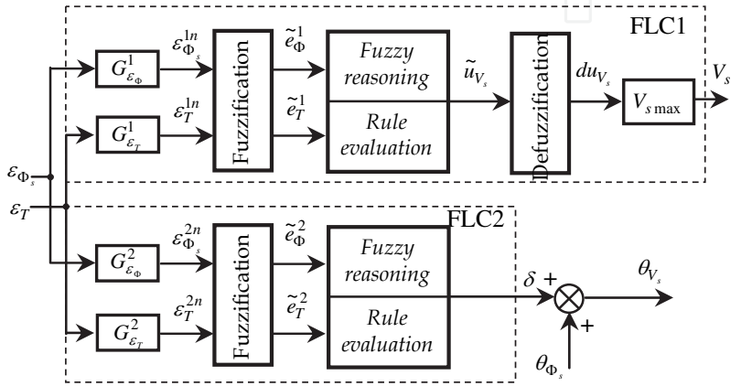

Fig. 11. Fuzzy logic controller structure

$\tilde{e}_T$ / $\tilde{e}_\Phi$	NG	NM	NP	EZ	PP	PM	PG
NG	PG	PM	PP	PP	PP	PM	PG
NM	PG	PM	PP	PP	PP	PM	PG
NP	PG	PM	PP	EZ	PP	PM	PG
EZ	PG	PM	PP	EZ	PP	PM	PG
PP	PG	PM	PP	EZ	PP	PM	PG
PM	PG	PM	PP	PP	PP	PM	PG
PG	PG	PM	PP	PP	PP	PM	PG

Table 1. FLC 1 rules

$\varepsilon_{\Phi_S}^n$	P			Z			N		
ε_T^n	P	Z	N	P	Z	N	P	Z	N
δ	$\frac{\pi}{4}$	0	$\frac{-\pi}{4}$	$\frac{\pi}{2}$	$\frac{\pi}{2}$	$\frac{-\pi}{2}$	$\frac{3\pi}{2}$	π	$\frac{-3\pi}{4}$

Table 2. Reference voltage increment angle

3.2 PI resistance estimator for PMSM-fuzzy DTC drive

The system diagram can be shown in Fig. 11. It is seen that the input to the PI resistance estimator is torque and flux reference, together with the stator current. Rotor position is not needed for the PI estimator (Mir, 1998; Hartani, 2010).

When the stator resistance changes, the compensation process will be applied. Therefore, the change of stator resistance will change the amplitude of the current vector. So, the error between the amplitude of current vector and that of the reference current vector will be used to compensate the change in stator resistance until the error becomes zero.

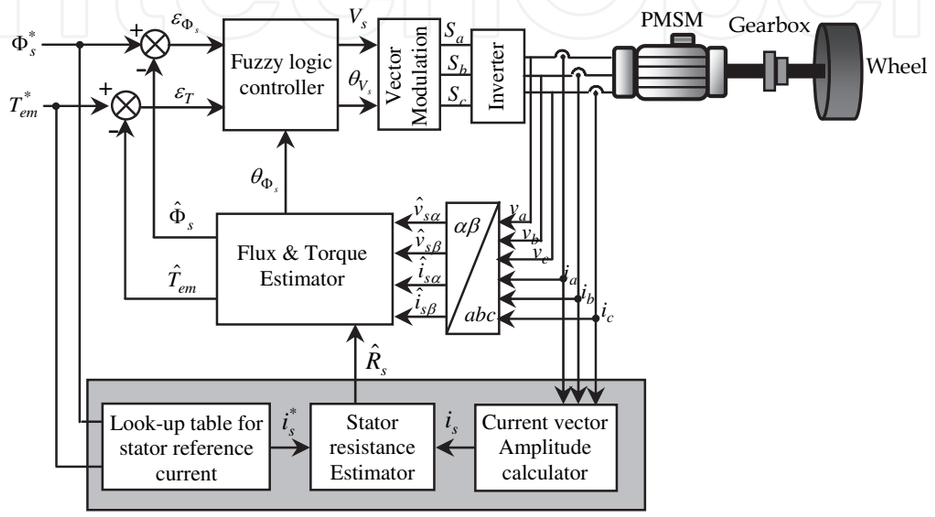

Fig. 12. System diagram of a PMSM-fuzzy DTC drive system with stator PI resistance estimator

Based on the relationship between change of resistance and change of current, a PI resistance estimator can be constructed by Eq. (15), as shown in Fig. 13. Here, i_s^* is the current vector corresponding to the flux and torque, and i_s is the measured stator current vector.

$$\Delta R_s = \left(kp + \frac{ki}{s} \right) \Delta i_s \tag{15}$$

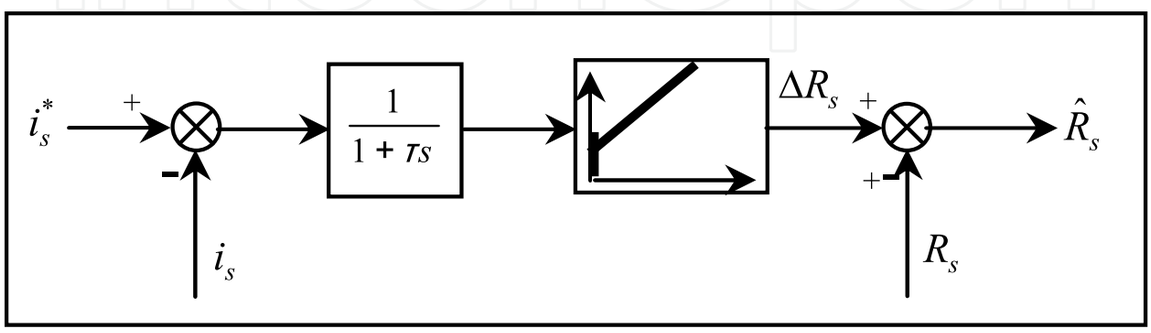

Fig. 13. PI resistance estimator for FDTC-PMSM drive system

3.2.1 Amplitude of stator reference current

The PMS machine's torque and flux vector are given by (16) and (17) in the vector reference frame. The amplitude of flux vector can be calculated using (19).

$$T_{em} = \frac{3}{2} p\left[\Phi_f i_q - \left(L_q - L_d\right) i_d i_q\right] \tag{16}$$

$$\begin{cases} \Phi_d = L_d i_d + \Phi_f \\ \Phi_q = L_q i_q \end{cases} \tag{17}$$

$$\left|\Phi_s\right| = \sqrt{\Phi_d^2 + \Phi_q^2} \tag{18}$$

The reference torque and flux are given, respectively, by:

$$\begin{cases} T_{em}^* = \frac{3}{2} p\left[\Phi_f i_q^* - \left(L_q - L_d\right) i_d^* i_q^*\right] \\ \left|\Phi_s^*\right| = \sqrt{\left(L_d i_d^* + \Phi_f\right)^2 + \left(L_q i_q^*\right)^2} \end{cases} \tag{19}$$

The stator current amplitude is obtained using the relation given by:

$$\left|i_s^*\right| = \sqrt{i_d^{*2} + i_q^{*2}} \tag{20}$$

A Matlab/Simulink model was built in order to verify the performance of the PI resistance estimator. The system performances with and without the resistance estimator were then compared. Fig. 14 shows the result of flux, torque, and amplitude of current of the system with PI stator resistance estimator.

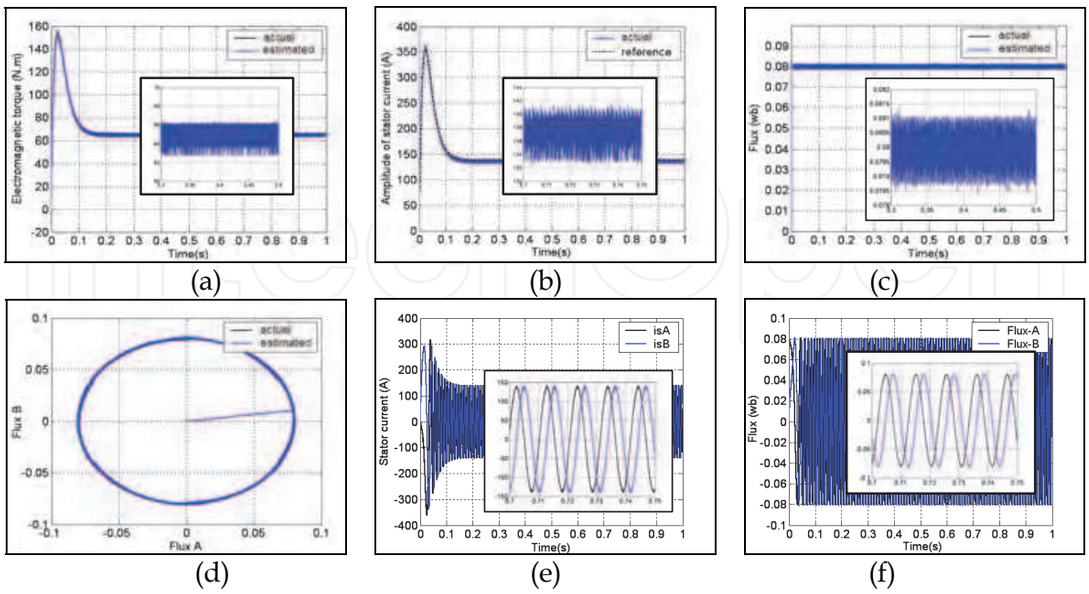

Fig. 14. Performances of the FDTC-PMSM drive system with a ramp-up in stator resistance with compensation

3.3 Maximum control structure

The maximum control structure (MCS) is obtained systematically by applying the principles of inversion to the model EMR of the process (Bouscayrol, 2002). We define by this method the control structure relating to the mechanical model of the vehicle. In our application, the variable to be controlled is the vehicle speed by acting on the motor torques of both wheels. The maximum control structure is shown in Fig. 15, by taking into account only one wheel for simplification.

This structure shows the problems involved in the inversions of the mechanical coupling by the accumulation element and of non-linearity relating to the contact wheel-road.

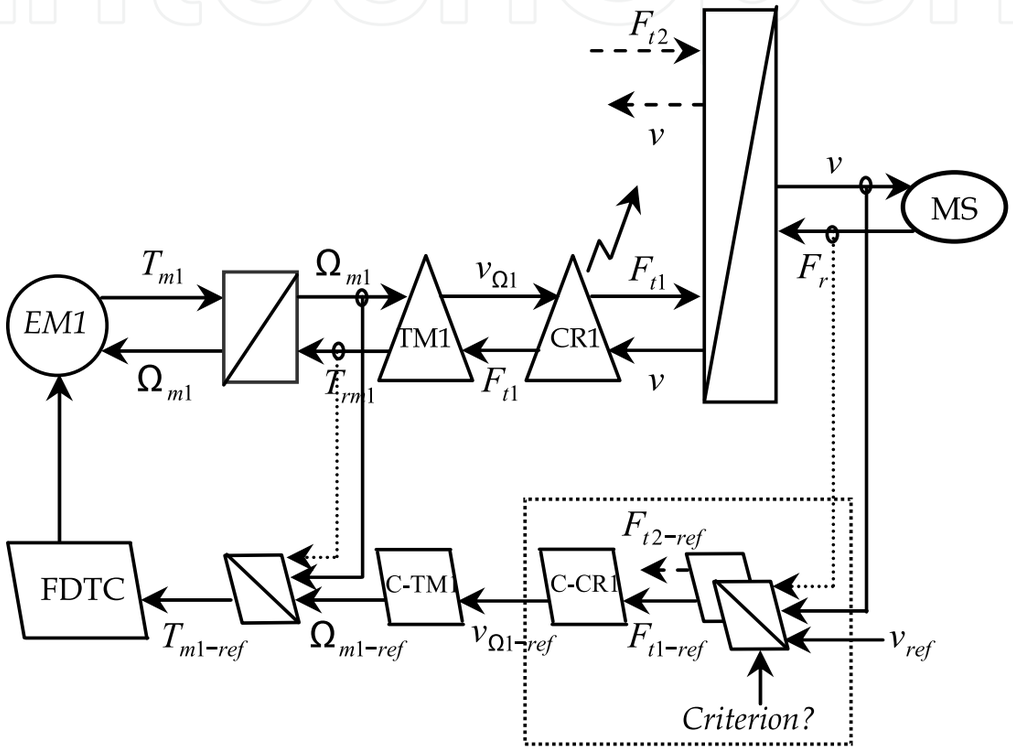

Fig. 15. EMR of the maximum control of the vehicle

3.3.1 Inversion of the coupling by accumulation elements

The inversion of the relation (15) shows that this control is done by controlling a traction effort ($F_{t1} + F_{t2}$) where each wheel contributes to the advance of the vehicle. However, the inversion of the COG requires the use of a controller where the ergonomic analyzes showed that the driver wishes to keep the control of traction effort by acting on an accelerator pedal in order to control the vehicle speed. In this work, we admit that the action of the driver provides the reference of the total traction effort $(F_{t1} + F_{t2})_{ref}$, Fig. 16. The difficulty of this reference is how to distribute the forces between both wheels (F_{t1-ref} and F_{t2-ref}). The solution of this difficulty can be solved by adding a condition to the inversion of the rigid relation. This condition ($F_{t1-ref} = F_{t2-ref}$) is relating to the stability of the vehicle to imbalance the forces transmitted to each wheel which is closer to the equivalent torques imposed by the classical mechanical differential.

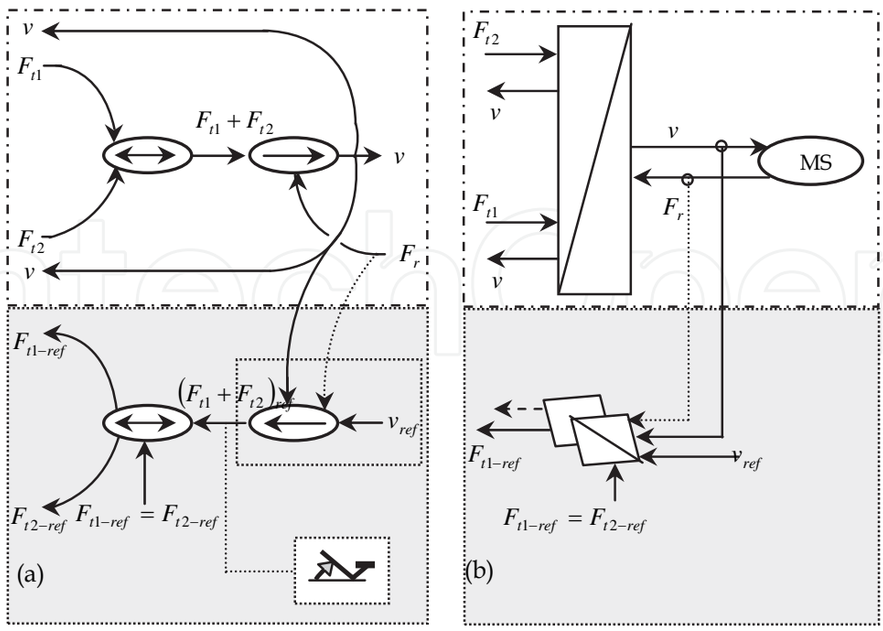

Fig. 16. Modulation of the traction effort: (a) COG and (b) EMR.

3.3.2 Inversion of the converter CR

We should now define the speed of each wheel in order to ensure the balance of the traction forces. However, the problems which we will face are the nonlinearity and the badly known of the relation to reverse which depends of the road conditions. In the following work, we propose two methods to solve these problems.

3.4 Anti skid strategy by slip control

The proposed solution will be obtained from the maximum control structure, Fig. 15. In this case, the solution to be used to reverse the converter CR is based on the principle of inversion of a badly known rigid relation. We can now apply with this type of relation, the principles of inversion of a causal relation which will minimize the difference between the output and its reference by using a classical controller. The principle of this strategy is based on Fig. 17.

3.4.1 Inversion of relation CR1

Figure 18, shows the COG inversion of relation CR1. We need now the measurements or estimations of the variables speed and traction effort of each wheel.

The linear velocity estimation permits a true decoupling in the control of both wheels (Pierquin, 2001) and the definition of the reference speed which is given by the following equation:

$$v_{\Omega 1\_ref} = \frac{v}{1 - \lambda_{1\_ref}} \tag{22}$$

In the control structure, the maximum slip is limited to 10% which constitutes the real function anti skidding.

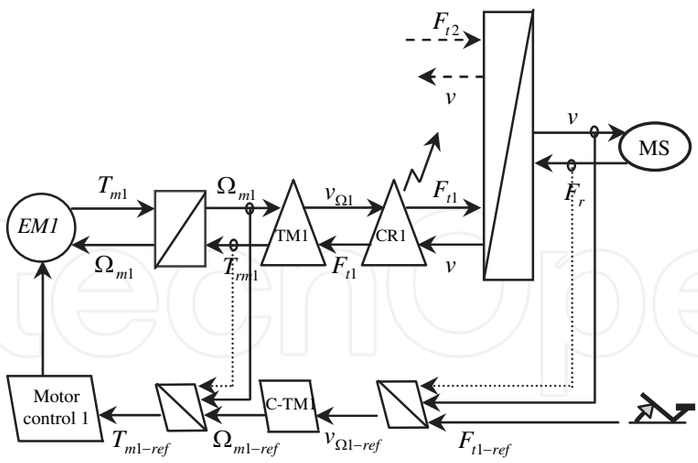

Fig. 17. Control structure deduced from the inversion

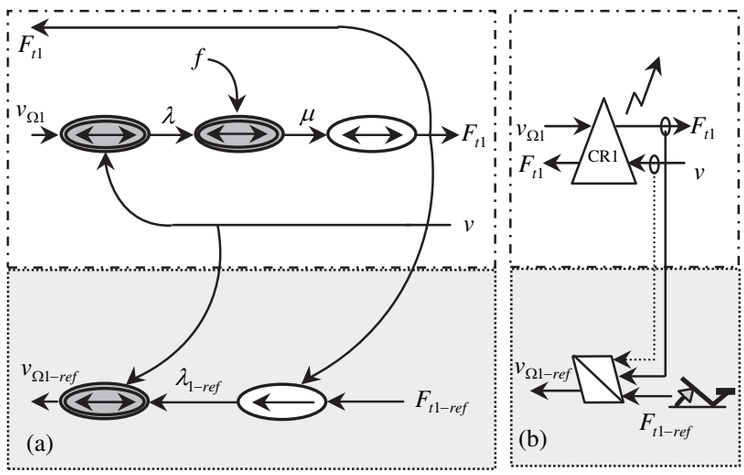

Fig. 18. Inversion of the converter CR: (a) COG; (b) EMR

3.5 Anti skid strategy by BMC

3.5.1 The BMC structure

The behaviour model control (BMC) can be an alternative to other robust control strategies. It is based on a supplementary input of the process to make it follow the model (Hautier, 1997 ; Vulturescu, 2000; Pierquin, 2000).

The process block correspondens to the real plant, Fig. 19. It can be characterised by its input vector u and its output vector y.

The control block has to define an appropriated control variable u, in order to obtain the desired reference vector y_{ref}.

The model block is a process simulation. This block can be a simplified model of the process. The difference between the process output y and the model output y_{mod} is taken into account by the adaptation block. The output of this block acts directly on the process by a supplementary input, Fig. 19. The adaptation mechanism can be a simple gain or a classical controller (Vulturescu, 2004).

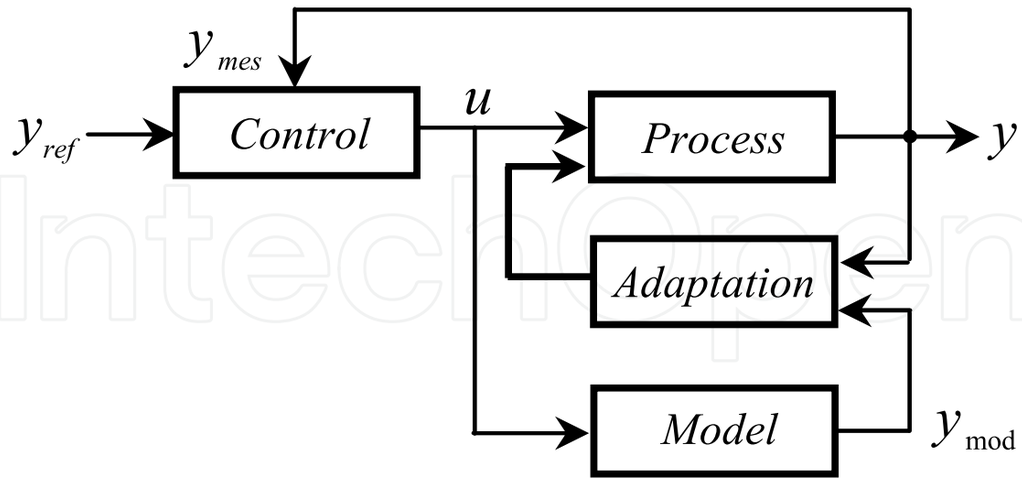

Fig. 19. Example of a BMC structure

3.5.2 Application of the BMC control to the traction system

The first step to be made is to establish a behaviour model. In this case, we choose a mechanical model without slip, which will be equivalent to the contact wheel-road in the areas known as pseudo-slip. This model can be considered as an ideal model. However, the inertia moments of the elements in rotation and the vehicle mass can be represented by the total inertia moments J_{t_mod} of each shaft motor which is given by:

$$J_{t\_\mathrm{mod}} = \tilde{J}_{\Omega} + \tilde{M}\left(\tilde{k}_{red}\tilde{r}\right)^2 \tag{23}$$

The dynamic equation of the model is given by:

$$J_{t\_\mathrm{mod}} \frac{d\Omega_{\mathrm{mod}}}{dt} = T_{m\_\mathrm{mod}} - T_{rm\_\mathrm{mod}} \tag{24}$$

By taking into account the wheel slip, the total inertia moments will become:

$$J_t = J_{\Omega} + M(1-\lambda)\left(k_{red}r\right)^2 \tag{25}$$

We now apply the BMC structure for one wheel to solve the skid phenomenon described before. In Fig. 20, we have as an input the reference torque and as an output the speed of the motor which drives the wheel. However, the main goal of this structure of control is to force the speed Ω_m of the process to track the speed Ω_{m_mod} of the model by using a behaviour controller.

It was shown that the state variables of each accumulator are not affected with the same manner by the skid phenomenon. The speed wheel is more sensitive to this phenomenon than that of vehicle in a homogeneous ratio to the kinetic energies, Fig. 5(a). Hence, the motor speed is taken as the output variable of the model used in the BMC control. The proposed control structure is given by Fig. 20.

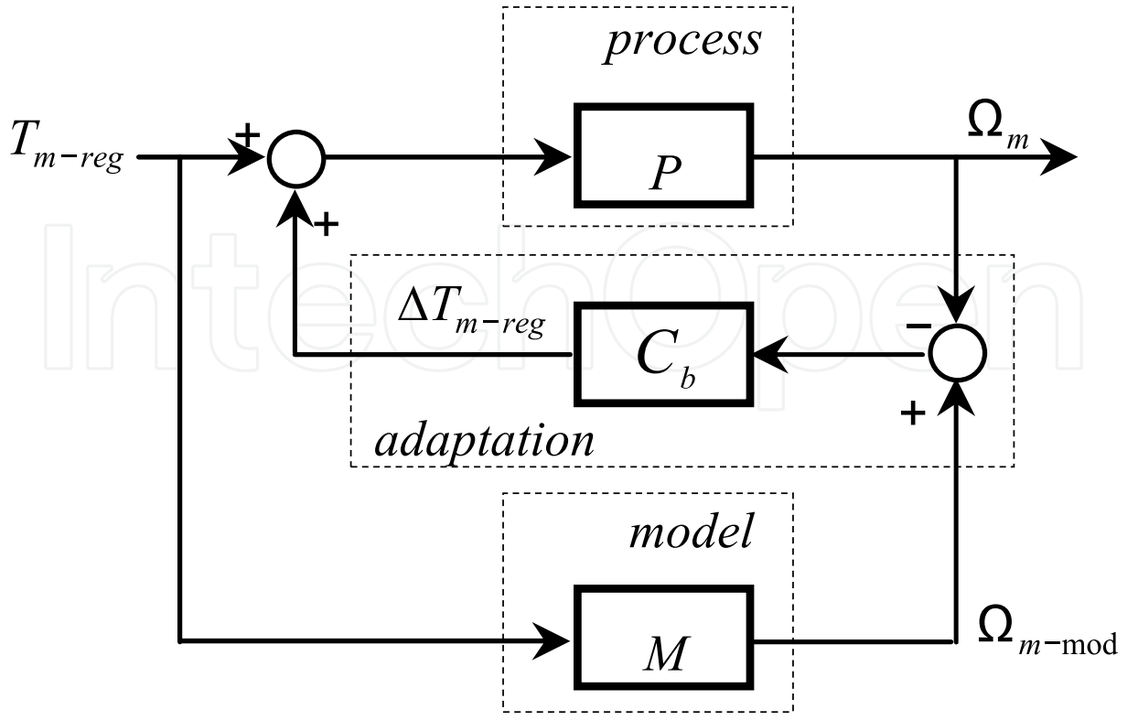

Fig. 20. BMC control applied to one wheel

The influence of the disturbance on the wheel speeds in both controls is shown in Fig. 21. An error is used to compare the transient performances of the MCS and the BMC. This figure shows clearly that the perturbation effect is negligible in the case of BMC control and demonstrates again the robustness of this new control.

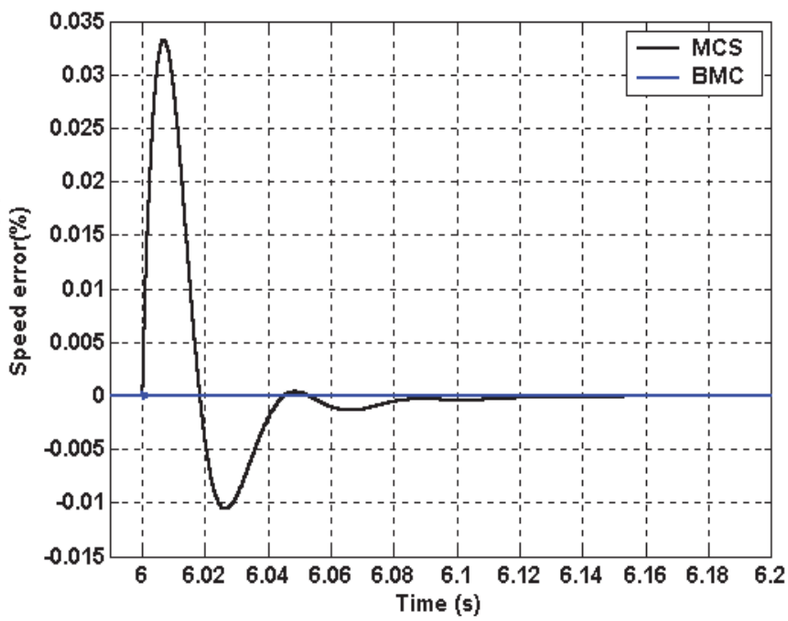

Fig. 21. Effect of a loss of adherence of MCS and BMC controls

4. Simulation results

We have simulated by using different blocks of Matlab/Simulink the proposed traction system. This system is controlled by the behaviour model control (BMC) based on the DTC strategy applied to each motor, Fig. 20, for the various conditions of environment (skid phenomenon), Fig. 22.

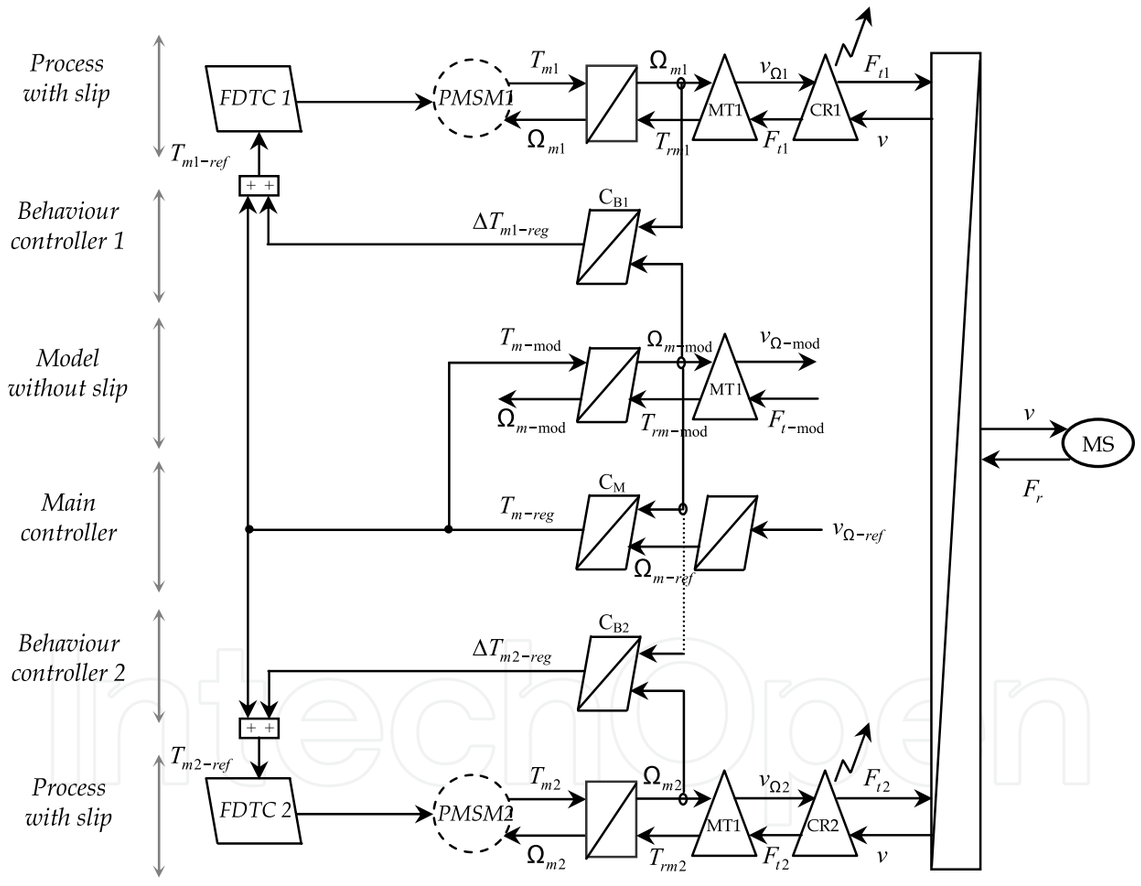

Fig. 22. BMC structure applied to the traction system

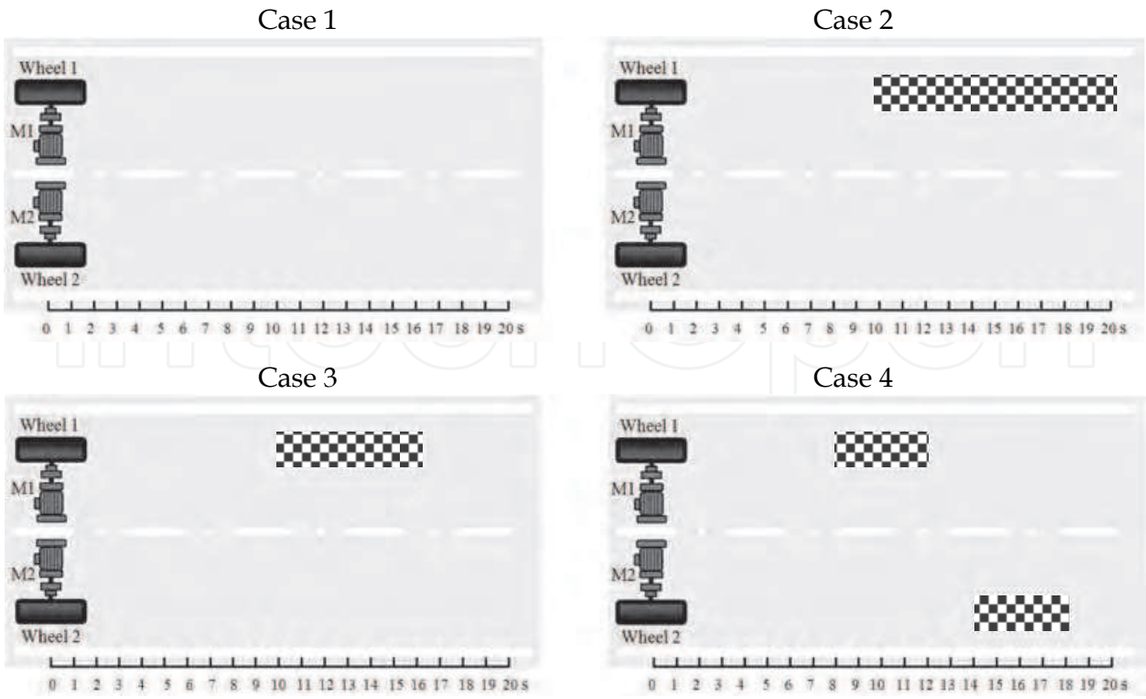

Fig. 23. Simulation cases. Dry road Slippery road

4.1 Case 1

Initially, we suppose that the two wheels are not skidding and are not disturbed. Then, a 80 *km/h* step speed is applied to our system. We notice that the speeds of both wheels and vehicle are almost identical. These speeds are illustrated in the Fig. 24(a) and (b). Fig. 24(c) shows that the two motor speeds have the same behaviour to its model. The difference between these speeds is represented in the Fig. 24(d). From Fig. 24(e) we notice that the slips λ_1 and λ_2 of both wheels respectively, are maintained in the adhesive region and the traction forces which are illustrated by the Fig. 24(f) are identical, due to the same conditions taken of both contact wheel-road. The motor torques are represented in Fig. 24(g) and the imposed torques of the main controller and the behaviour controllers are shown in Fig. 24(h). The resistive force of the vehicle is shown by the Fig. 24(i).

4.2 Case 2

We simulate now the system by using the BMC control and then applying a skid phenomenon at $t = 10s$ to wheel 1 which is driven by motor 1 when the vehicle is moving at a speed of $80km/h$. The skidding occurs when moving from a dry road ($\mu_1(\lambda)$) to a slippery road ($\mu_2(\lambda)$) which leads to a loss of adherence.

The BMC control has a great effect on the adaptation blocks and by using the behaviour controllers to maintain permanently the speed of the vehicle and those of the wheels close to their profiles, Fig. 25(a). However, both driving wheel speeds give similar responses as shown in Fig. 25(b).

Figure 25(c) shows that the two motor speeds have the same behaviour with the model during the loss of adherence. The difference between these speeds which is negligible is represented in the Fig. 25(d).

The loss of adherence imposed on wheel 1 results to a reduction in the load torque applied to this wheel, consequently its speed increases during the transient time which induces a small variation of the slip on wheel 2, Fig. 25(e). The effect of this variation, leads to a temporary increase in the traction force, Fig. 18(i). However, the BMC control establishes a self-regulation by reducing the electromagnetic torque T_{m1} of motor 1 and at the same time increases the electromagnetic torque T_{m2} to compensate the load torque of motor 2, Fig. 25(j) and Fig. 25(k). Figures 25(n) and 25(o) show the phase currents of motor 1 and motor 2 respectively.

4.3 Case 3

In this case, the simulation is carried out by applying a skid phenomenon between $t = 10s$ and $t = 16s$ only to wheel 1.

As shown in Fig. 26(i). and during the loss of adherence, the traction forces applied to both driving wheels have different values. At $t = 16s$, when moving from a slippery road ($\mu_2(\lambda)$) to a dry road ($\mu_1(\lambda)$), the BMC control establishes a self-regulation by increasing the electromagnetic torque T_{m1} of motor 1 and at the same time decreases the electromagnetic torque T_{m2} of motor 2, Fig. 26(j) and (k) which results to a negligible drop of speeds, Fig. 26(d), (e) and (f).

4.4 Case 4

The simulation is carried out by applying a skid phenomenon to both wheels successively at different times. Figure 27(c) shows that the two motor speeds have the same behaviour to the model. The difference between these speeds is represented in the Fig. 27(g).

When the adherence of the wheel decreases, the slip increases which results to a reduction in the load torque applied to this wheel. However, the BMC control reduces significantly the speed errors which permits the re-adhesion of the skidding wheel. Therefore, it is confirmed that the anti-skid control could maintain the slip ratio around its optimal value, Fig. 27(h).

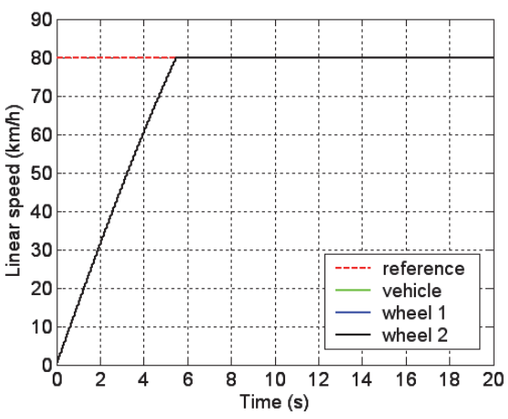

(a)

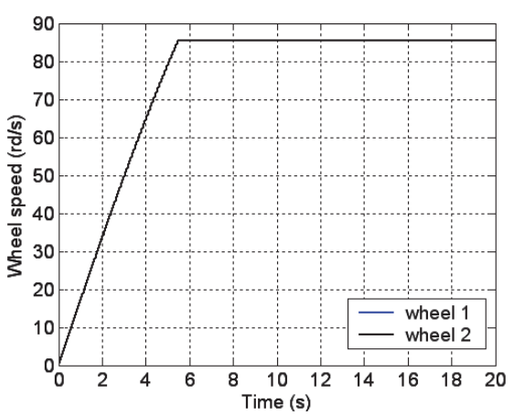

(b)

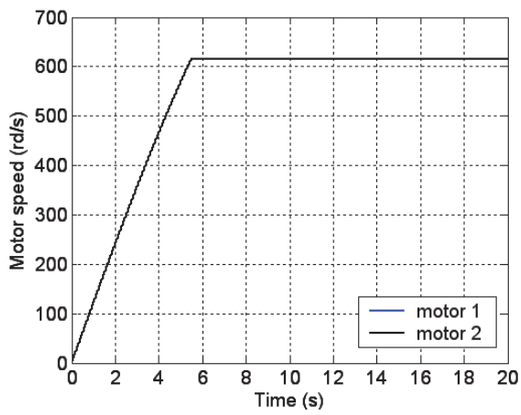
Motor speed (rd/s)
Time (s)
motor 1
motor 2

(c)

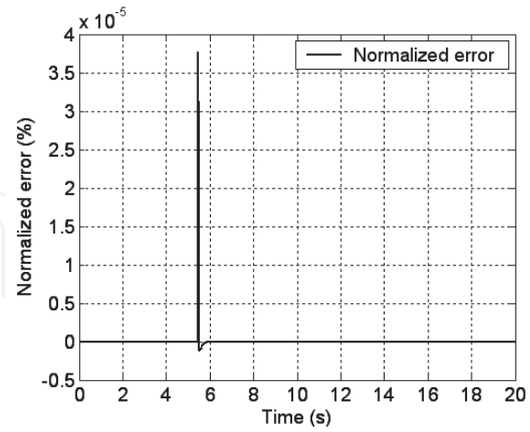
x 10^-5
Normalized error
Normalized error (%)
Time (s)

(d)

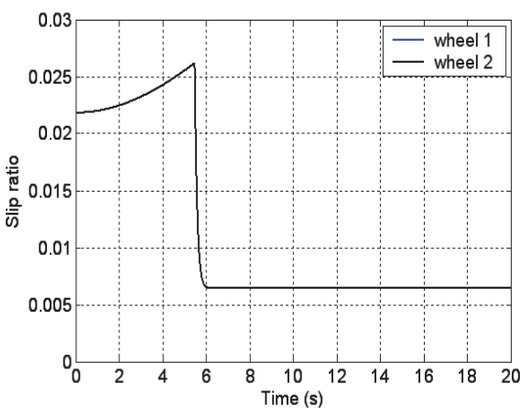
wheel 1
wheel 2
Slip ratio
Time (s)

(e)

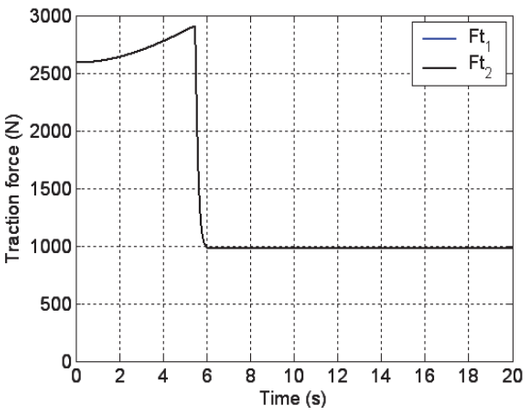
Ft1
Ft2
Traction force (N)
Time (s)

(f)

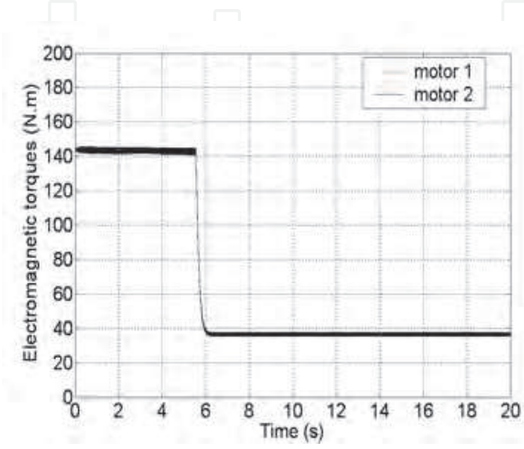
motor 1
motor 2
Electromagnetic torques (N.m)
Time (s)

(g)

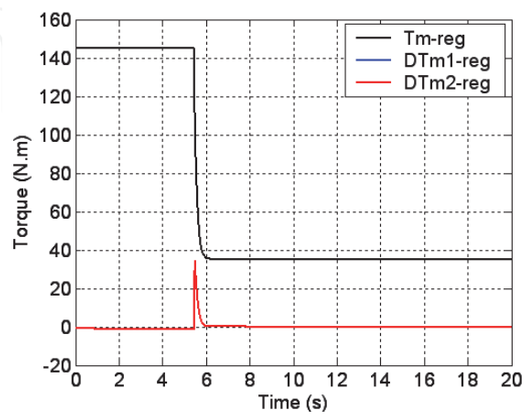
Tm-reg
DTm1-reg
DTm2-reg
Torque (N.m)
Time (s)

(h)

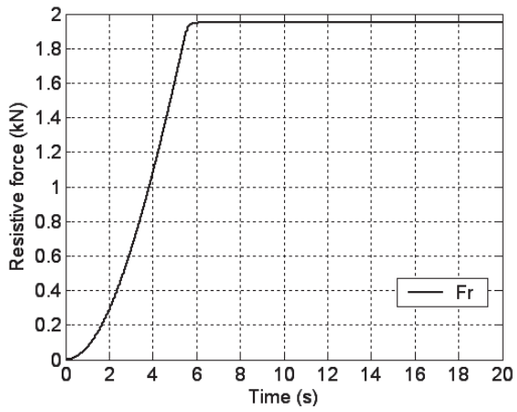

(i)

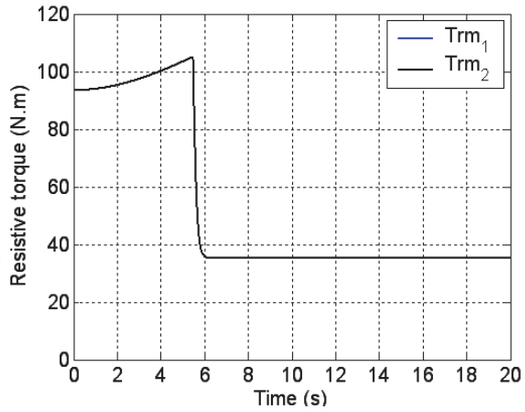

(j)

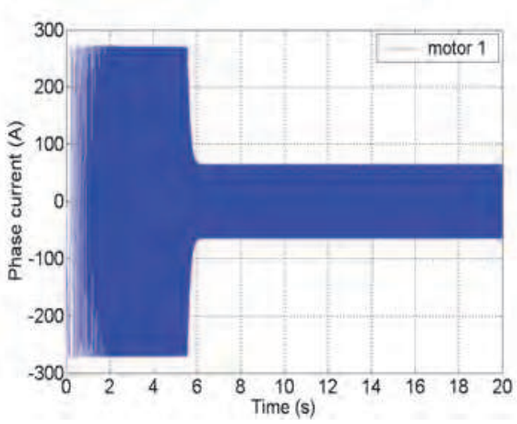

(k)

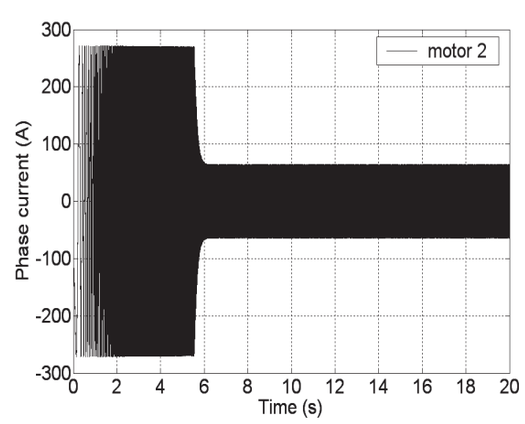

(l)

Fig. 24. Simulation results for case 1

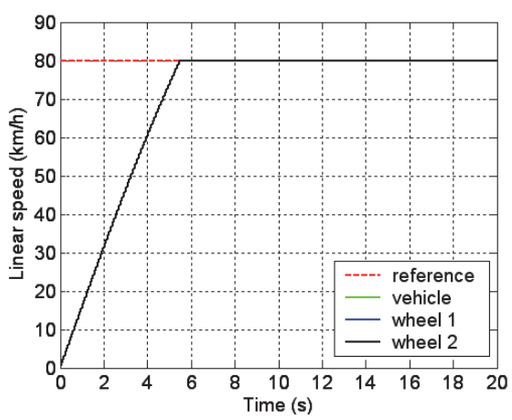

(a)

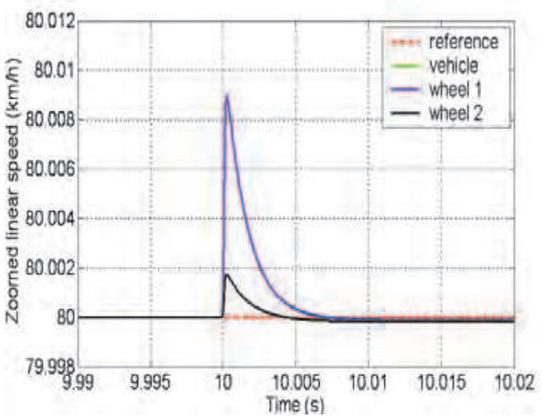

(b)

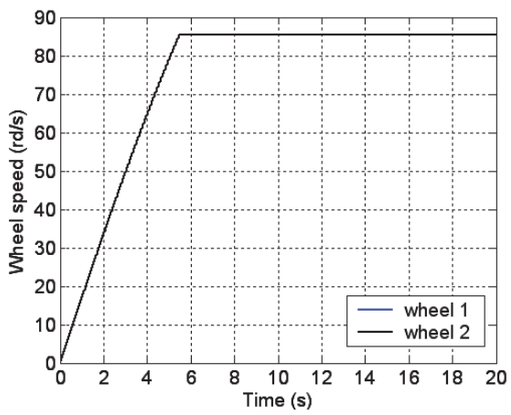
Wheel speed (rd/s)
Time (s)
wheel 1
wheel 2

(c)

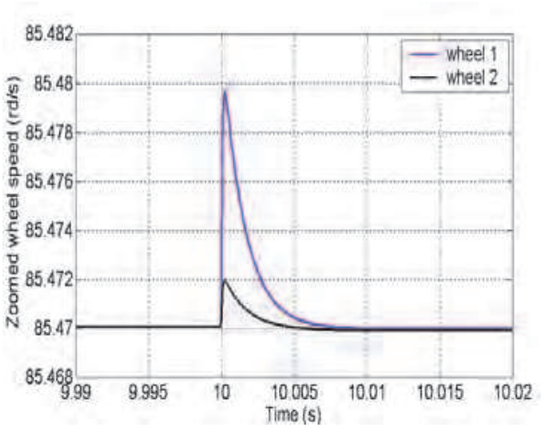
Zoomed wheel speed (rd/s)
Time (s)
wheel 1
wheel 2

(d)

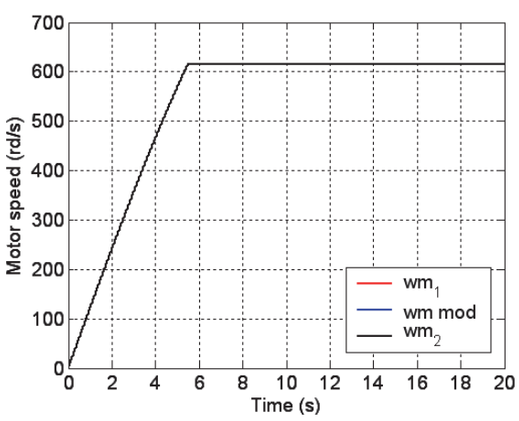
Motor speed (rd/s)
Time (s)
wm1
wm mod
wm2

(e)

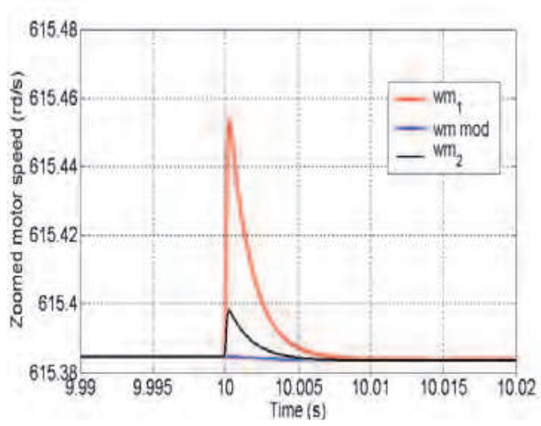
Zoomed motor speed (rd/s)
Time (s)
wm1
wm mod
wm2

(f)

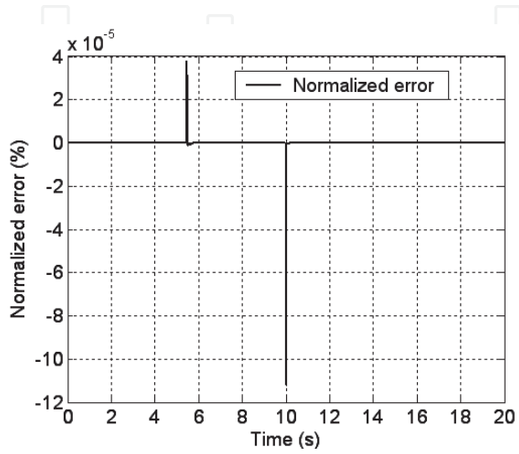
x 10^-5
Normalized error
Normalized error (%)
Time (s)

(g)

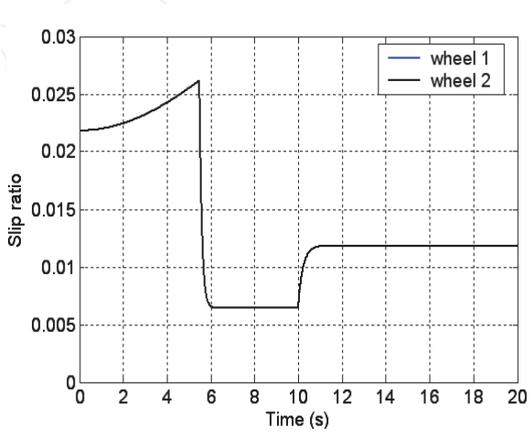
Slip ratio
Time (s)
wheel 1
wheel 2

(h)

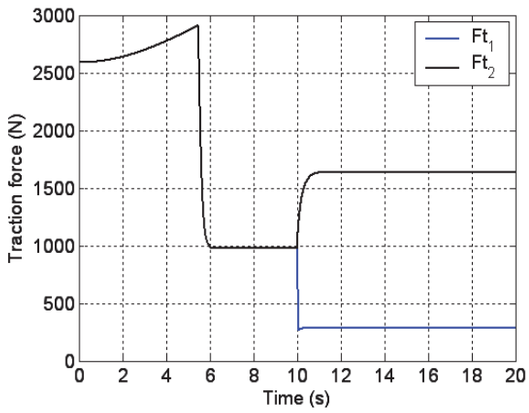
Traction force (N)
Time (s)
Ft1
Ft2

(i)

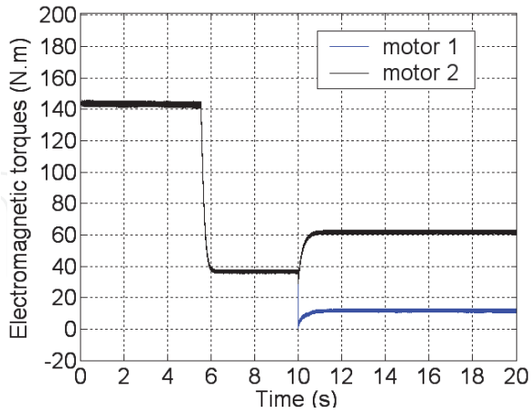
Electromagnetic torques (N.m)
Time (s)
motor 1
motor 2

(j)

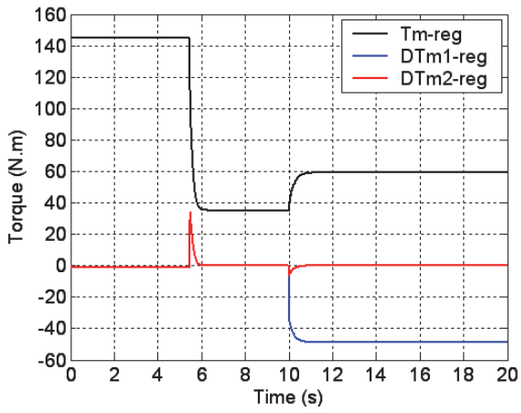
Torque (N.m)
Time (s)
Tm-reg
DTm1-reg
DTm2-reg

(k)

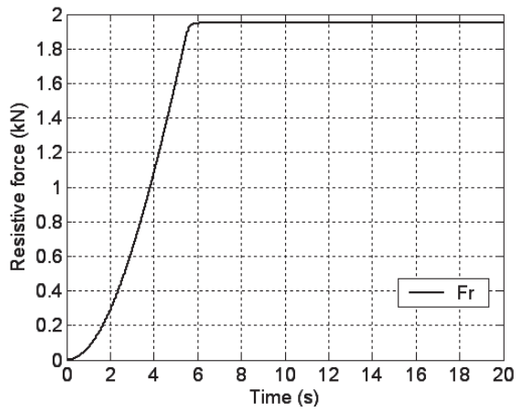
Resistive force (kN)
Time (s)
Fr

(l)

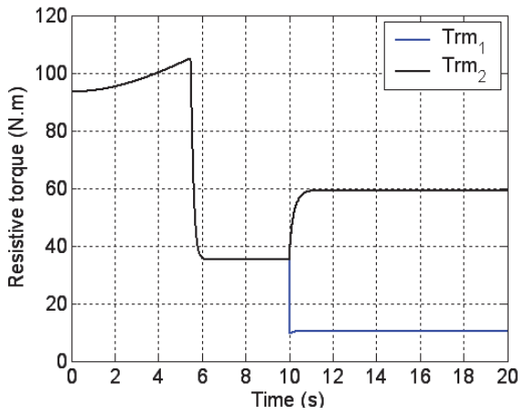
Resistive torque (N.m)
Time (s)
Trm1
Trm2

(m)

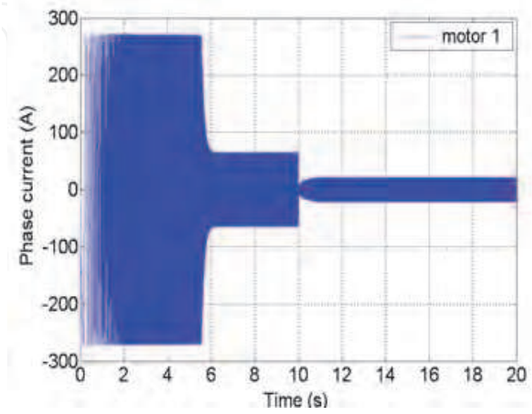
Phase current (A)
Time (s)
motor 1

(n)

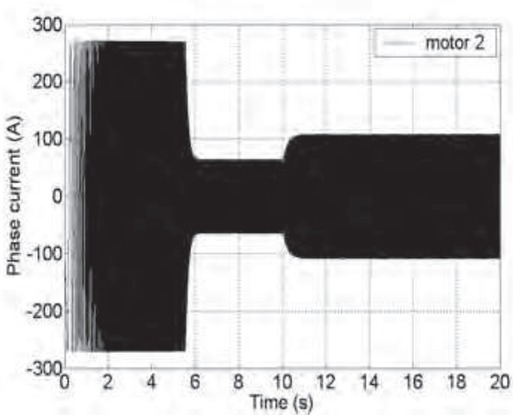

(o)

Fig. 25. Simulation results for case 2

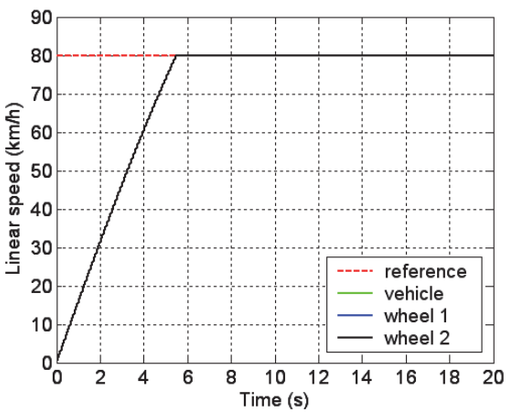

(a)

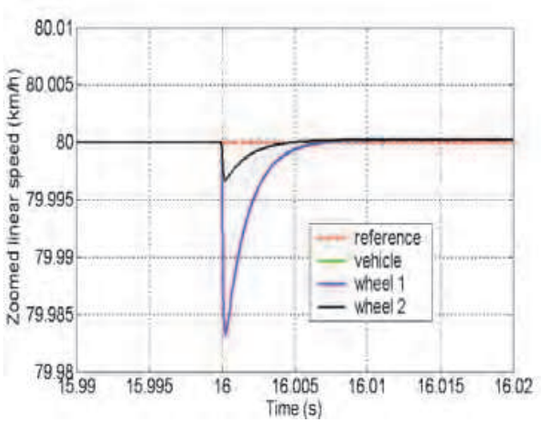

(b)

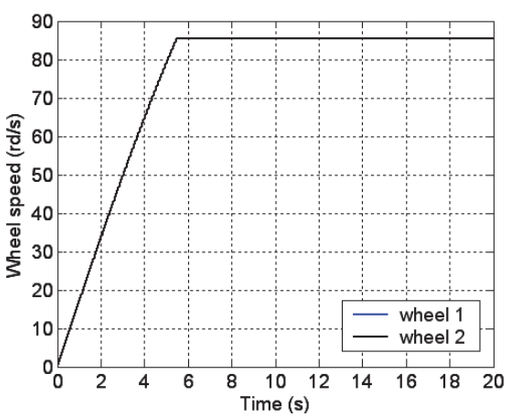

(c)

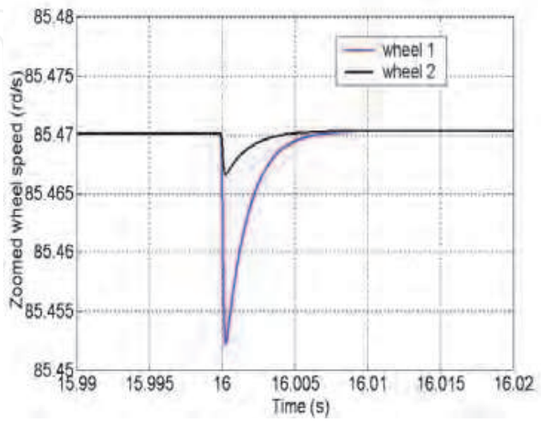

(d)

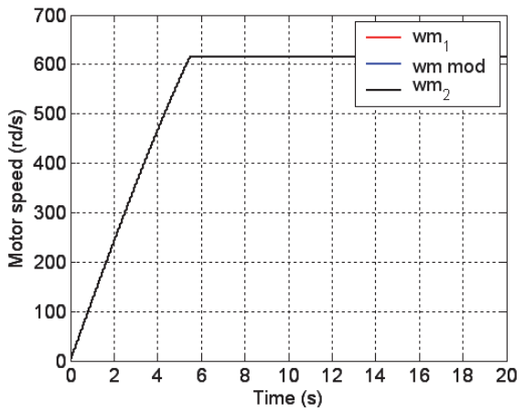
Motor speed (rd/s)
Time (s)
wm1
wm mod
wm2

(e)

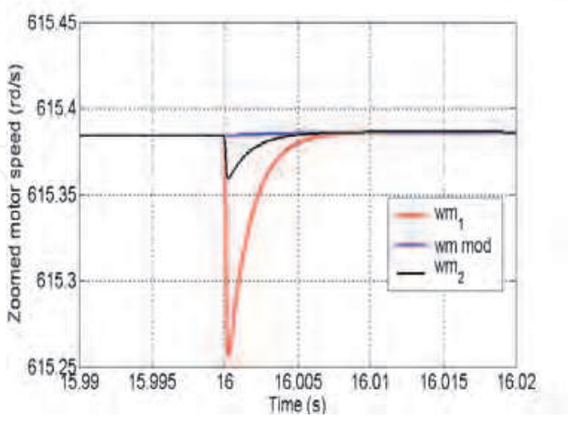
Zoomed motor speed (rd/s)
Time (s)
wm1
wm mod
wm2

(f)

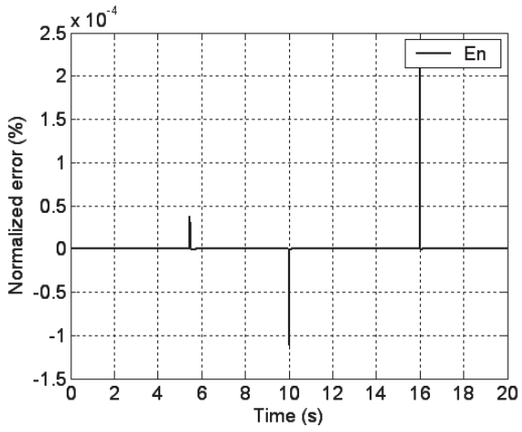
x 10-4
Normalized error (%)
Time (s)
En

(g)

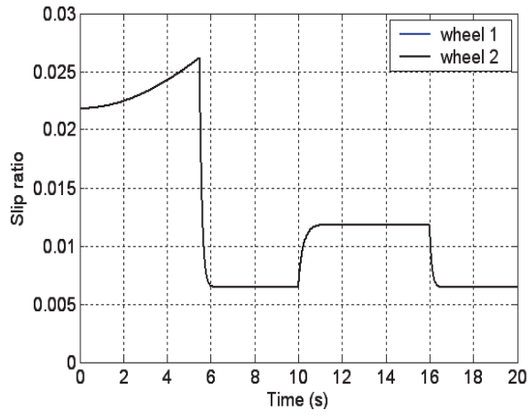
Slip ratio
Time (s)
wheel 1
wheel 2

(h)

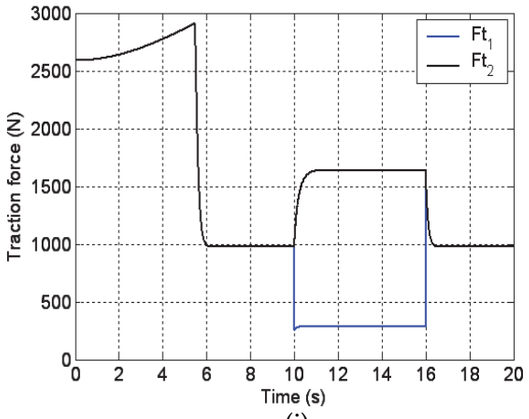
Traction force (N)
Time (s)
Ft1
Ft2

(i)

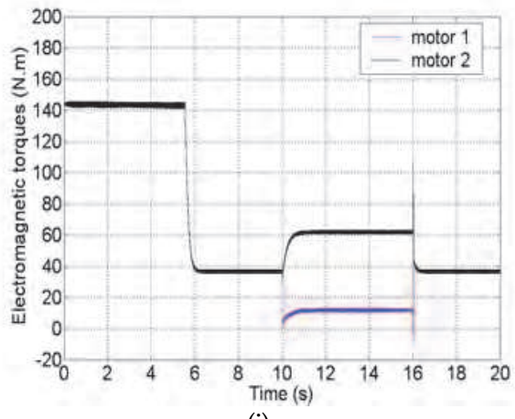
Electromagnetic torques (N.m)
Time (s)
motor 1
motor 2

(j)

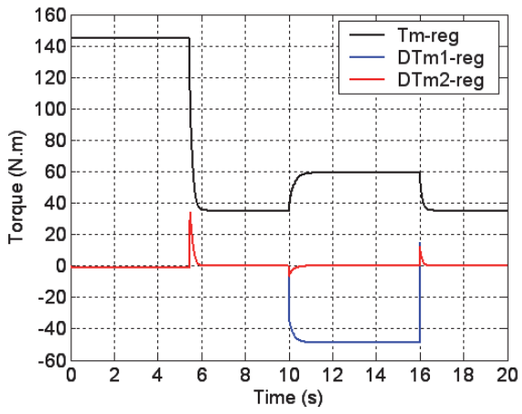

(k)

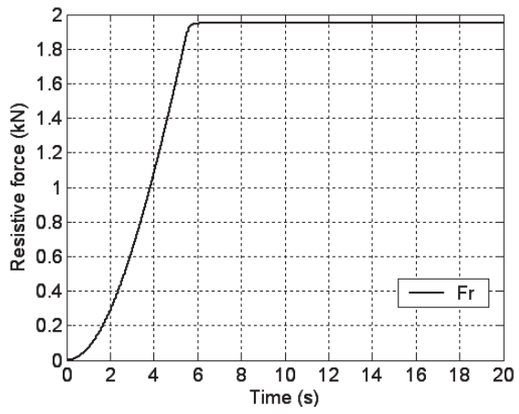

(l)

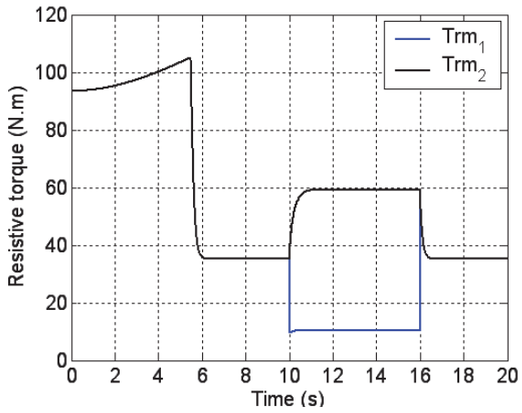

(m)

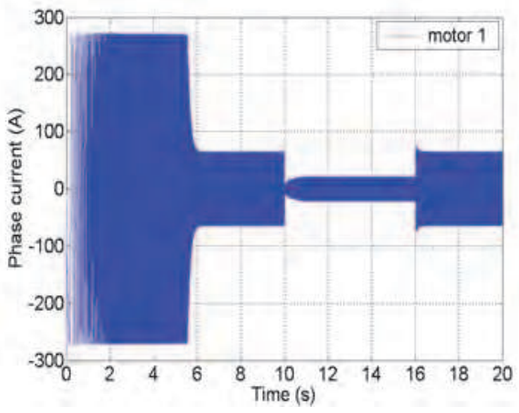

(n)

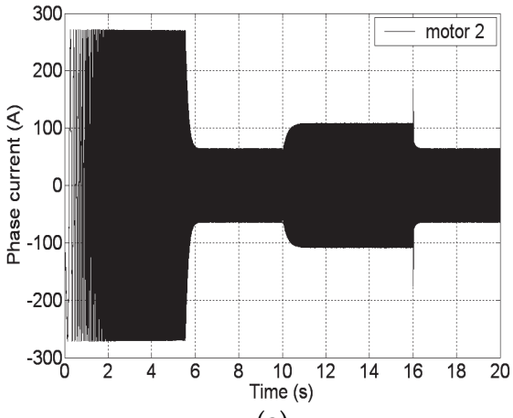

(o)

Fig. 26. Simulation results for case 3

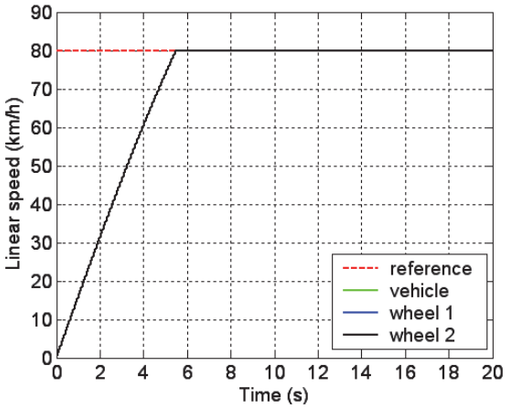
Linear speed (km/h)
Time (s)
reference
vehicle
wheel 1
wheel 2

(a)

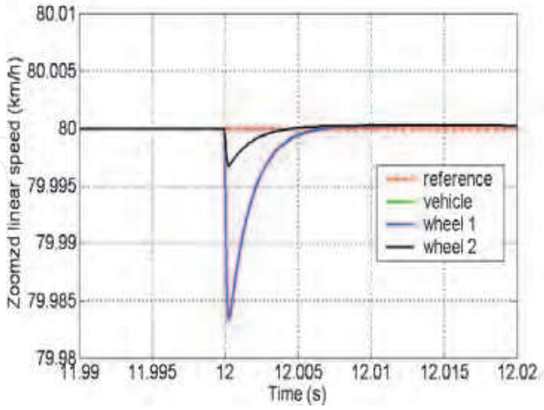
Zoomzd linear speed (km/h)
Time (s)
reference
vehicle
wheel 1
wheel 2

(b)

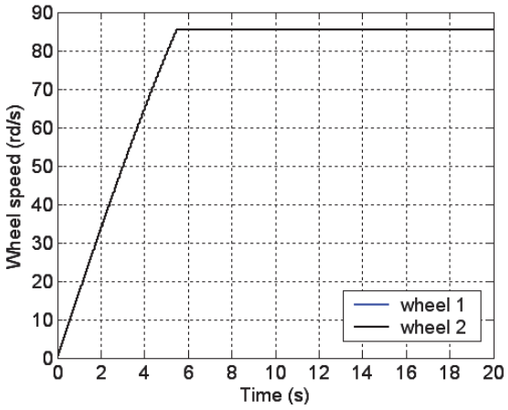
Wheel speed (rd/s)
Time (s)
wheel 1
wheel 2

(c)

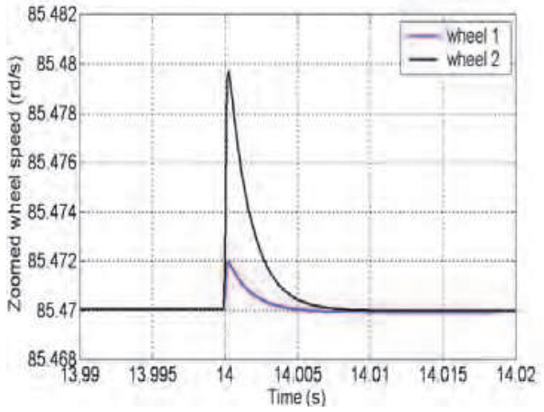
Zoomed wheel speed (rd/s)
Time (s)
wheel 1
wheel 2

(d)

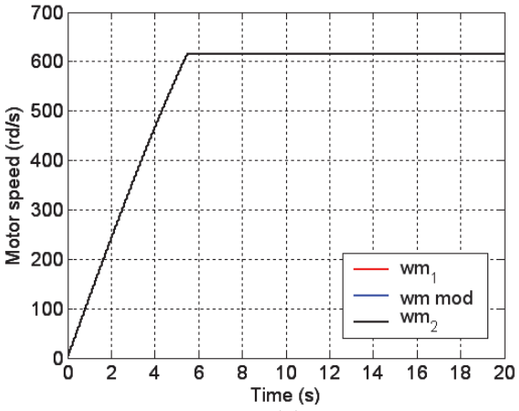
Motor speed (rd/s)
Time (s)
wm1
wm mod
wm2

(e)

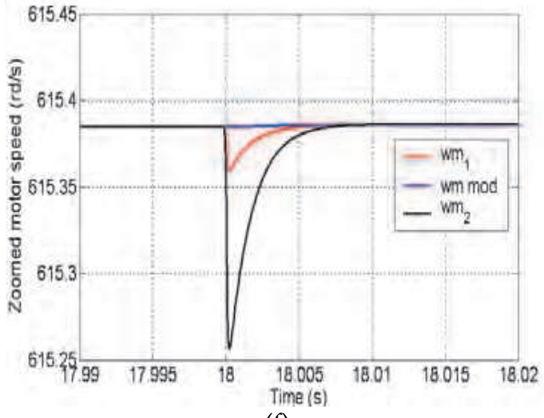
Zoomed motor speed (rd/s)
Time (s)
wm1
wm mod
wm2

(f)

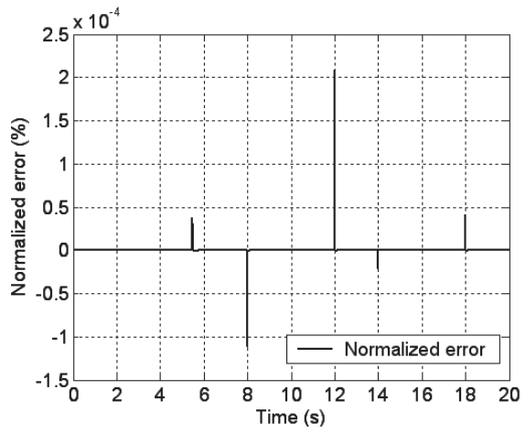
x 10^-4
Normalized error (%)
Time (s)
Normalized error

(g)

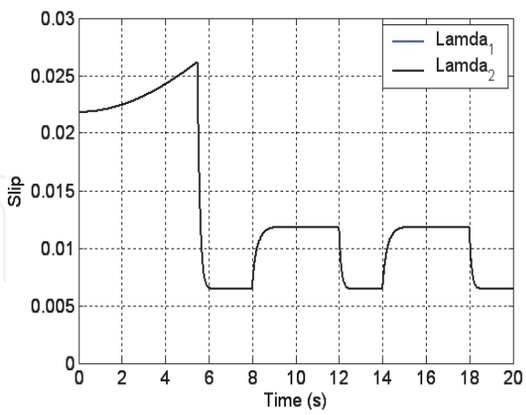
Slip
Time (s)
Lamda1
Lamda2

(h)

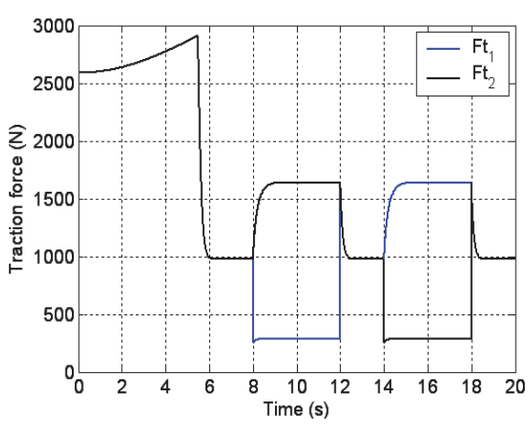
Traction force (N)
Time (s)
Ft1
Ft2

(i)

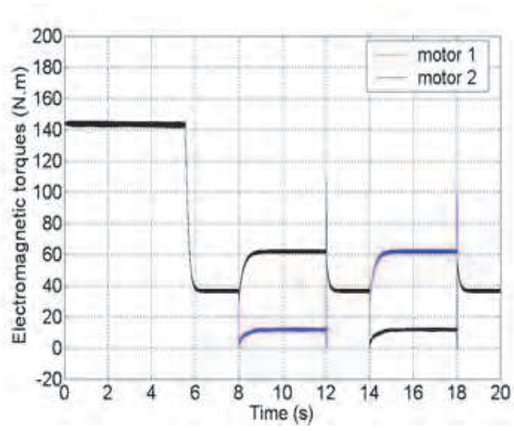
Electromagnetic torques (N.m)
Time (s)
motor 1
motor 2

(j)

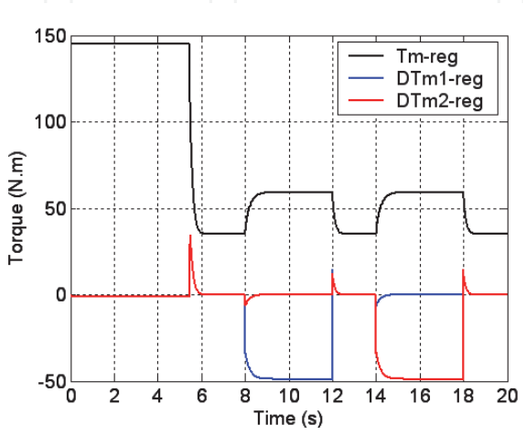
Torque (N.m)
Time (s)
Tm-reg
DTm1-reg
DTm2-reg

(k)

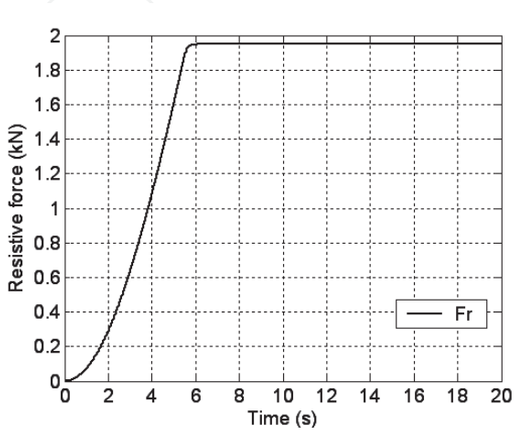
Resistive force (kN)
Time (s)
Fr

(l)

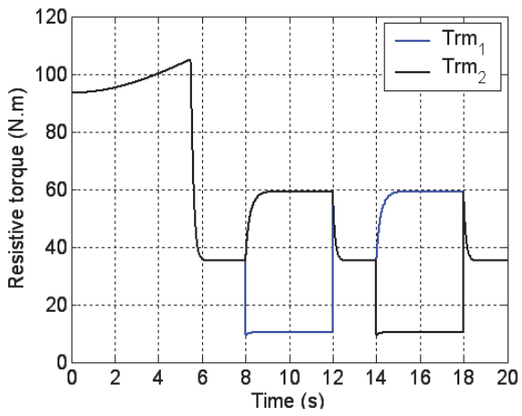

(m)

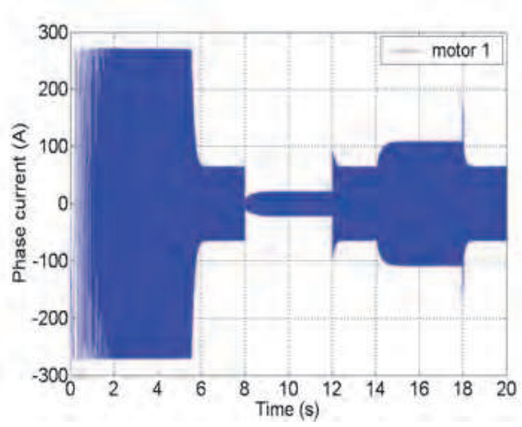

(n)

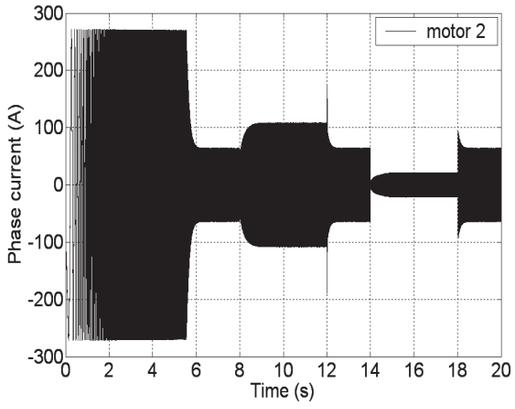

(o)

Fig. 27. Simulation results for case 4

5. Conclusion

In this chapter, a new anti-skid control for electric vehicle is proposed and discussed. This work contributes to the improvement of the electric vehicle stability using behaviour model control. According to the results obtained by simulations for all the cases, the proposed traction system shows a very stable behaviour of the electric vehicle during the various conditions of adherence.

6. Abbreviations

COG : Causal Ordering Graph
DTFC : Direct Torque Fuzzy Control
EC : Electrical Coupling
EM : Electrical machine

EMR : Energetic Macroscopic Representation
ES : Electrical Source
EV : Electric Vehicle
MC : Mechanical Coupling
MCS : Maximum Control Structure
MMS : Multi-machine Multi-converter Systems
MS : Mechanical Source
PMSM : Permanent Magnet synchronous Machine
SC : Static converter

7. Appendix

Parameter	Symbol	Unit	Value
Vehicle total mass	M	Kg	1200
Wheel radius	r	m	0,26
Aerodynamic drag coefficient	C_D	N/(ms)2	0,25
Vehicle frontal area	S	m²	1,9
Gearbox ratio	k_{red}	–	1/7,2
Efficiency of the gearbox	η	–	0,98

Table 3. The Specifications of the Vehicle Used in Simulation

Parameter	Symbol	Unit	Value
Resistance	R	Ω	0,03
d -axis inductance	L_d	H	2.10^{-4}
q -axis inductance	L_q	H	2.10^{-4}
Permanent magnet flux	Φ_f	Wb	0,08
Pole pairs	p	–	4

Table 4. The specifications of motors

8. References

Bouscayrol, A.; Davat, B.; de Fornel, B.; François, B.; Hautier, J.P.; Meibody-Tabar, F.; Monmasson, E.; Pietrzak-David, M.; Razik, H.; Semail, E.; Benkhoris, F. (2003), Control structures for multi-machine multi-converter systems with upstream coupling. *Elsevier, Mathematics and computers in simulation* Vol. 63, pp. 261-270, 2003.

Bouscayrol, A.; Davat, B.; de Fornel, B.; François, B.; Hautier, J.P.; Meibody-Tabar, F.; Pietrzak-David, M. (2000), Multi-machine multi-converter systems for drives: analysis of couplings by a global modelling. *in: Proceedings of the IEEE-IAS Annual Meeting, Rome*, October 2000.

Arnet, B.; Jufer, M. (1997), Torque control on Electric vehicles with separate wheel drives. *Proceeding of EPE'97,* Trondhein, Vol. 4, pp. 39-40, 1997.

Hartani, K.; Bourahla, M.; Mazari, B. (2005), New driving wheels control of electric vehicle, *Journal of Electrical Engineering*, Vol. 5, pp. 36-43.

Hartani, K.; Bourahla, M.; Miloud, Y. (2007), Electric vehicle with two independent wheel drive – Performance improvement by an electronic differential using sliding-mode control, *Electromotion*, Vol. 14, No. 2, pp. 99-113.

Merciera, J.C.; Verhille, J.N.; Bouscyrol, A. (2004), Energetic Macroscopic Representation of a subway traction system for a simulation model, *IEEE-ISIE'04,* Ajaccio (France), Vol. 2, pp. 1519–1524, May 2004.

Pragasen, P.; Krishnan, R. (1989), Modeling, Simulation, and Analysis of Permanent Magnets Motor Drives, Part I: The Permanent Magnets Synchronous Motor Drive, *IEEE Transactions on Industry Applications,* 25 (2), 265-273.

Miloudi, A.; Eid, A.; Al-radadi, A.; Draou, D. (2007), A variable gain PI controller used for speed control of a direct torque neuro fuzzy controlled induction machine drive, *Turk. J. Elec. Engin*. Vol. 15 No. 1, pp. 37-49.

Miloudi, A.; Eid, A.; Al-radadi, A.; Draou A.; Miloud, Y. (2004), Simulation and modelling of a variable gain PI controller for speed control of a direct torque neuro fuzzy controlled induction machine drive, in proc. *PESC'04*, Aechan, Germany, June. 20-25, pp. 3493-3498.

Tang, L.; Zhang, L.; Rahman, M. F.; Yumen, Hu. (2004), A novel direct torque controlled interior permanent magnet synchronous machine drive with low ripple in flux and torque and fixed frequency, *IEEE Trans. on Power Electronics*, Vol. 19, No. 2, pp. 346-354.

Sun, D.; Yikang, He.; Zhu, J. G. (2004), Fuzzy logic direct torque control for permanent magnet synchronous motors, *Proc. Of the 5th world congress on intelligent control and automation*, Hanzzhou, P.R. China, June 15-19, 2004.

Gustafsson, F. (1998), Monotiring tire-road friction using the wheel slip," *IEEE Control Systems Magazines*. Vol.18, No.4, pp. 42-49, 1998.

Gustafsson, F. (1997), Slip based tire-road friction estimation, *Automatica*. Vol.33, No.6, pp. 1087-1099, 1997.

Hori, Y.; Toyoda, Y.; Tsuruoka, Y. (1998), Traction control of electric vehicule based on the estimation of road surface condition. Basic experimental results using the test EV

"UOT electric march, *IEEE. Trans. on Industry Applications*. Vol. 34, No.5, pp. 1131-1138, 1998.

Guillaud, X.; Degobert, P.; Hautier, J.P. (2000), Modeling, control and causality: the causal ordering graph," *16th IMACS world congress*, CD-ROM, Lausanne, Switzerland; August 2000.

Ehsani, M.; Rahman, K. M.; Toliyat, H.A. (1997), Propulsion system design and Hybrid vehicles," *IEEE Transactions on Industrial Electronics*, Vol. 44, No.1, pp.19-27, 1997.

Wong, J. Y. (1993), The theory of ground vehicle, *Wiley–Interscience Publication* 1993, ISBN 0-471-58496-4.

Bouscayrol, A.; Delarue, Ph. (2002), Simplifications of the Maximum Control Structure of a wind energy conversion system with an induction generator, *Int. J. Renew Energy Eng*., Vol.4, no.2, pp. 479–485, 2002.

Pierquin, J.; Vulturescu, B.; Bouscayrol, A.; Hautier, J. P. (2001), Behaviour model control structures for an electric vehicle, *EPE'2001*, CD-ROM, Graz (Austria), August, 2001.

Hautier, J.P.; Garon, J.P. (1997), Systèmes automatiques, *Tome 2, Commande de processus, Edition Ellipses*, Paris, 1997.

Vulturescu, B.; Bouscayrol. A.; Hautier, J.P.; Guillaud, X.; Ionescu, F. (2000), Behaviour model control of a DC machine, *ICEM2000, Conference Espoo* (Finland). August 2000.

Pierquin, J.; Escane, P.; Bouscayrol, A.; Pietrzak-David, M.; Hautier, J.P.; de Fornel, B. (2000), Behaviour model control of a high speed railway traction system, *EPE-PEMC 2000 Conference*, Kocise (Slovak Republic), Vol. 6, pp. 197-202, September 2000.

Vulturescu, B.; Bouscayrol, A.; Ionescu, F.; Hautier, J.P. (2004), Behaviour model control for cascaded processes: Application to an electrical drive, *Elsevier, Computers and Electrical Engineering,* vol.30, pp. 509-526, 2004.

Sado, H.; Sakai, S., Hori, Y. (1999), Road condition estimation for traction control in electric vehicle, *In Proc. IEEE Int. Symp. Industrial Electronic*, Solvenia, pp. 973-978, 1999.

Okano, T.; Tai, C.; Inoue, T.; Uchida, T.; Sakai, S., Hori, Y. (2002), Vehicle stability improvement Based on MFC independently installed on 4 wheels-Basic experiments using "UOT Electric March II", *In proc. PCC-Osaka*, Vol. 2, pp. 582-587, 2002.

Sakai, S.; Hori, Y. (2001), Advantage of electric motor for antiskid control of electric vehicle, *EPE Journal*, Vol. l.11, No.4, pp. 26-32, 2001.

Takahachi, I.; Noguchi, T. (1986), A new quick-response and high-efficiency control strategy of an induction motor, *IEEE Trans. Ind. Applicat.,* Vol. 22, No. 5, pp. 820-827, 1986.

French, C.; Acarnley, P. (1996), Direct torque control of permanent magnet drives, *IEEE Trans. Ind. Appl*. Vol. 32, No. 5, pp. 1080-1088, Sep./Oct. 1996.

Vyncke, T.J.; Melkebeek, J. A.; Boel, R. K. (2006), Direct torque control of permanent magnet synchronous motors - an overview, *in conf.Proc. 3rd IEEE Benelux Young Research Symposium in Electrical Power Engineering,* No. 28, Ghent, Begium, Apr. 27-28, p.5, 2006.

Vasudevan, M.; Arumugam, R. (2004), New direct torque control scheme of induction motor for electric vehicles, *5th Asian* Control Conference, Vol. 2, 20-23, pp. 1377 – 1383, 2004.

Mir, S.; Elbuluk, M. E.; Zinger, D. S. (1998), PI and Fuzzy Estimators for Tuning the stator resistance in direct torque control of induction machines, *IEEE Transactions Power Electronics*, Vol. 13, No. 2, pp. 279 – 287, March, 1998.

Hartani, K.; Miloud, Y.; Miloudi, A. (2010), Improved Direct Torque Control of Permanent Magnet Synchronous Electrical Vehicle Motor with Proportional-Integral Resistance Estimator, *Journal of Electrical Engineering & Technology*, Vol. 5, N°3, pp. 451-461, September 2010, ISSN 1975-0102.

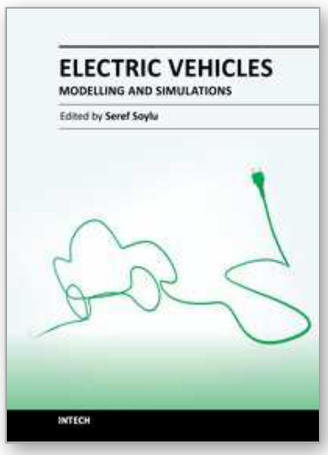

Electric Vehicles - Modelling and Simulations

Edited by Dr. Seref Soylu

ISBN 978-953-307-477-1
Hard cover, 466 pages
Publisher InTech
Published online 12, September, 2011
Published in print edition September, 2011

In this book, modeling and simulation of electric vehicles and their components have been emphasized chapter by chapter with valuable contribution of many researchers who work on both technical and regulatory sides of the field. Mathematical models for electrical vehicles and their components were introduced and merged together to make this book a guide for industry, academia and policy makers.

InTech Europe
University Campus STeP Ri
Slavka Krautzeka 83/A
51000 Rijeka, Croatia
Phone: +385 (51) 770 447
Fax: +385 (51) 686 166
www.intechopen.com

InTech China
Unit 405, Office Block, Hotel Equatorial Shanghai
No.65, Yan An Road (West), Shanghai, 200040, China
中国上海市延安西路65号上海国际贵都大饭店办公楼405单元
Phone: +86-21-62489820
Fax: +86-21-62489821

IntechOpen